Heat Generation Measurements of Prismatic Lithium Ion Batteries

by

Kaiwei Chen

A thesis
presented to the University of Waterloo
in fulfilment of the
thesis requirement for the degree of
Master of Applied Science
in
Mechanical Engineering

Waterloo, Ontario, Canada, 2013

I hereby declare that I am the sole author of this thesis. This is a true copy of the thesis, including any required final revisions, as accepted by my examiners.

I understand that my thesis may be made electronically available to the public.

Abstract

Electric and hybrid electric vehicles are gaining momentum as a sustainable alternative to conventional combustion based transportation. The operating temperature of the vehicle will vary significantly over the vehicle lifetime and this variance in operating temperature will strongly impact the performance, driving range, and durability of batteries used in the vehicles.

In the first part of this thesis, an experimental facility is developed to accurately quantify the effects of battery operating temperature on discharge characteristics through precise control of the battery operating temperatures, utilizing a water-ethylene glycol solution in a constant temperature thermal bath. A prismatic 20Ah $LiFePO_4$ battery from A123 is tested using the developed method, and temperature measurements on the battery throughout discharge show a maximum variation of 0.3°C temporally and 0.4°C spatially at a 3C discharge rate, in contrast to 13.1°C temperature change temporally and 4.3°C spatially when using the conventional air convection temperature control method under the same test conditions. A comparison of battery discharge curves using the two methods show that the reduction in spatial and temporal temperature change in the battery has a large effect on the battery discharge characteristics. The developed method of battery temperature control yields more accurate battery discharge characterization due to both the elimination of state-of-charge drift caused by spatial variations in battery temperature, and inaccurate discharge characteristics due to battery heat up at various discharge and ambient conditions. Battery discharge characterization performed using the developed method of temperature control exhibits a reduction in battery capacity of 95% when the operating temperature is decreased from 20°C to -10°C at 3C discharge rate. A reduction of 35% in battery capacity is observed when for the same temperature decrease at a 0.2C discharge rate. The observed effect of operating temperature on the capacity of the tested battery highlights the importance of an effective thermal management system, the design of which requires accurate knowledge of the heat generation characteristics of the battery under various discharge rates and operating temperatures.

In the second part of this thesis, a calorimeter capable of measuring the heat generation rates of a prismatic battery is developed and verified by using a controllable electric heater. The heat generation rate of a prismatic A123 $LiFePO_4$ battery is measured for discharge

rates ranging from 0.25C to 3C and operating temperature ranging from -10°C to 40°C. Results show that the heat generation rates of Lithium ion batteries are greatly affected by both battery operating temperature and discharge rate. At low rates of discharge the heat generation is not significant, even becoming endothermic at the battery operating temperatures of 30°C and 40°C. Heat of mixing is observed to be a non-negligible component of total heat generation at discharge rates as low as 0.25C for all tested battery operating temperatures. A double plateau in battery discharge curve is observed for operating temperatures of 30°C and 40°C. The developed experimental facility can be used for the measurement of heat generation for any prismatic battery, regardless of chemistries. The characterization of heat generated by the battery under various discharge rates and operating temperatures can be used to verify the accuracy of battery heat generation models currently used, and for the design of an effective thermal management system for electric and hybrid electric vehicles in the automotive industry.

Acknowledgements

I would like to thank my supervisor, Dr. Xianguo Li, for teaching me how to express myself effectively in technical writing, and for providing guidance and direction throughout my research. I would also like to thank Dr. Zhongwei Chen and Dr. Zhongchao Tan for taking the time to read and provide feedback on my thesis.

A sincere thank you to the members of our lab who were there to help me navigate the ups and downs of experimental research: Aaron Pereira, for all the advice and ideas you provided; Grant Unsworth, for all your help and advice on the design of the experiments, and the time spent discussing different ideas for this project.

Finally, thanks to Brian Kettlewell, for your insight and guidance on the complex world of mathematics.

This work is financially supported by the Ontario Research Fund-Research Excellence (ORF-RE) program via contract number # RE-02-019 and the Natural Sciences and Engineering Research Council of Canada (NSERC) via the Discovery Grant.

Dedication

To the one I love, who continues to show me the beauty of the world and the importance of achieving balance in life.

Table of Contents

List of Tables ix

List of Figures x

1 Introduction 1

1.1 Lithium Ion Batteries . . . 2

1.1.1 Lithium Ion Battery Components . . . 3

1.1.2 Electrochemical Mechanisms of the Lithium Ion Battery . . . 5

1.1.3 Types of Lithium Ion Batteries . . . 9

1.2 Motivation For This Work . . . 9

1.3 Scope and Outline of This Thesis . . . 11

2 Quantifying Temperature Effects on the Performance of Lithium Ion Batteries 13

2.1 Literature Review . . . 13

2.2 Experimental Setup . . . 17

2.3 Comparison of Battery Temperature Control Methods . . . 21

2.4 Effect of Operating Temperature on Battery Discharge Characteristics . . . 26

3 Calorimetric Measurements of Prismatic Li-ion Batteries 30

3.1 Literature Review . . . 30

3.2 Apparatus Design . . . 33

3.3 Experimental Condition and Procedure 39
3.4 Data Reduction 40
3.5 Calibration 45

4 Results and Discussion **48**
4.1 Effect of Discharge Rate on Heat Generation Rate 48
4.2 Effect of Operating Temperature on Heat Generation Rate 54
4.3 Validation of Results 58

5 Conclusions **61**
5.1 Summary 61
5.2 Recommendations 63

References **65**

Appendix A: Effect of Operating Temperature on Battery Discharge Curves **74**

Appendix B: Effect of Discharge Rate on Battery Heat Generation **78**

Appendix C: Effect of Operating Temperature on Battery Heat Generation **82**

List of Tables

1.1 Advantages and Disadvantages of Li-ion Batteries [67] 3

2.1 Spatial temperature variation of Li-ion batteries at various discharge rates at the end of the discharge process 15

2.2 Comparison of various test methods and their respective temporal temperature variations over the entire discharge cycles 16

2.3 Summary of test results for batteries at 20°C and various discharge rates, outlining the average temporal and spatial temperature variation for the discharge tests for both the water-ethylene glycol (WEG) and conventional air convection (air) temperature control methods 26

3.1 Accuracy and standard deviation of heat generation measured by battery calorimeter for varying operating temperatures 47

4.1 Summary of measured $LiFePO_4$ heat generation rates at all tested discharge rates and battery operating temperatures 60

List of Figures

1.1 Schematic of the electrochemical processes in a Li-ion cell [67] 6
1.2 Polarization curve of a battery, showing the effect of activation polarization, concentration polarization, and IR drop on open circuit voltage of a cell as a function of cell current [67] 8
1.3 A comparison of the internal setup of coin, cylindrical, and prismatic batteries [74] 10

2.1 Experimental setup for water-ethylene glycol (WEG) temperature control method 18
2.2 Thermocouple locations for battery temperature measurements (all measurements in mm). A total of 16 thermocouples were used, with 8 at corresponding locations on each side of the battery 19
2.3 Schematic of the conventional air convection temperature control method test setup 20
2.4 Test schedule used in the present study for Li-ion batteries at various discharge rates and operating temperatures 21
2.5 Comparison of the increase in battery temperature when discharging at 20°C using the conventional air convection (Air) temperature control method (the dashed curves) and the water-ethylene glycol (WEG) temperature control method (the solid curves) at 1C, 2C, and 3C discharge rate. 22
2.6 Comparison of standard deviations of battery temperature at 16 thermocouple locations (averaged over 5 repetitive tests) between the conventional air convection and water-ethylene glycol (WEG) temperature control method at 1C discharge rate and the set battery temperature of 20°C. 23

2.7 Comparison of battery discharge curves when discharging at 20°C using the conventional air convection (Air) temperature control method (the dashed curves) and the water-ethylene glycol (WEG) temperature control method (the solid curves) at 1C, 2C, and 3C discharge rate. 24
2.8 Battery discharge curves of the test battery at various temperatures for 3C discharge rate using the water-ethylene glycol temperature control method. 27
2.9 Relationship between battery energy and operating temperature for all discharge rates and temperatures tested 28

3.1 Exploded (left) and assembled (right) view of the experimental setup for the measurement of heat generation of prismatic Li-ion batteries. HDPE stands for high density polyethylene. 35
3.2 Schematic of the complete experimental setup. 36
3.3 Thermal resistivity measurements of the High Density Polyethylene slab . . 38
3.4 Test schedule used in the present study for charging and discharging of the Li-ion battery. 40
3.5 Problem setup for the measurement of inner temperature of the high density polyethylene (HDPE) slab T_{measured} from an imposed surface heat flux $\dot{q}''$ due to the heat generated in the test battery. 42
3.6 Comparison of the measured heat generation rate using Beck's Method (solid line) and the actual heat output from calibration heater (dashed line) at 10°C for a step down in heat output. Surface temperature refers to the temperature measured at the contact surface between the pseudo battery and the high density polyethylene (HDPE) slab. 46

4.1 Effect of tested discharge rates on the heat generation rate of an A123 $LiFePO_4$ battery at an operating temperature of 20°C. 49
4.2 Effect of discharge rate on the heat generation rate, non-dimensionalized by electrical power drawn, of A123 $LiFePO_4$ battery at an operating temperature of 20°C. 50
4.3 Effect of battery operating temperature on (a) heat generation rate and (b) battery discharge curve for an A123 $LiFePO_4$ battery at 0.5C discharge. . . 51

4.4 Battery discharge curve and measured heat generation profile of an A123 $LiFePO_4$ battery, for 1C discharge at 20°C. Measurements show the presence of additional heat generation post end of discharge. 52
4.5 Battery discharge curve and measured heat generation profile of an A123 $LiFePO_4$ battery, at 0.25C discharge, showing battery heat generation post the end of discharge for operating temperatures of (a) 40°C, and (b) -10°C. 53
4.6 Effect of battery operating temperature on (a) the heat generation rate and (b) the battery discharge curve of an A123 $LiFePO_4$ battery, for 1C discharge. 54
4.7 Heat generation rate of an A123 $LiFePO_4$ battery at (a) 40°C and (b) 0°C for all tested discharge rates. Secondary plateauing in heat generation rate at a depth of discharge of 0.8 can be observed for all discharge rates tested at 40°C. 56
4.8 Heat generation rates and battery discharge curves for 0.25C discharge at 30°C and 40°C. Transitions between voltage discharge curve plateaus correspond to regions of rapid change in the measured battery heat generation. 57
4.9 Comparison of the temperature measurements for the validation test and actual battery discharge for 1C, 2C and 3C discharge rates at an operating temperature of 20°C. 59

1 Effect of operating temperature on the discharge curve of the test battery at 0.25C constant current discharge 75
2 Effect of operating temperature on the discharge curve of the test battery at 0.5C constant current discharge 75
3 Effect of operating temperature on the discharge curve of the test battery at 1C constant current discharge 76
4 Effect of operating temperature on the discharge curve of the test battery at 2C constant current discharge 76
5 Effect of operating temperature on the discharge curve of the test battery at 3C constant current discharge 77
6 Effect of battery discharge rate on the heat generation profile of the test battery at an operating temperature of -10°C 79

7 Effect of battery discharge rate on the heat generation profile of the test battery at an operating temperature of 0°C 79
8 Effect of battery discharge rate on the heat generation profile of the test battery at an operating temperature of 10°C 80
9 Effect of battery discharge rate on the heat generation profile of the test battery at an operating temperature of 20°C 80
10 Effect of battery discharge rate on the heat generation profile of the test battery at an operating temperature of 30°C 81
11 Effect of battery discharge rate on the heat generation profile of the test battery at an operating temperature of 40°C 81
12 Effect of operating temperature on the heat generation profile of the test battery at 0.25C constant current discharge 83
13 Effect of operating temperature on the heat generation profile of the test battery at 0.5C constant current discharge 83
14 Effect of operating temperature on the heat generation profile of the test battery at 1C constant current discharge 84
15 Effect of operating temperature on the heat generation profile of the test battery at 2C constant current discharge 84
16 Effect of operating temperature on the heat generation profile of the test battery at 3C constant current discharge 85

Chapter 1

Introduction

Fossil fuel based transportation is one of the dominant contributors to global climate change and the main factor to increased urban air quality degradation. The growing public concern over climate change has propelled alternative forms of transportation to the forefront of research in the automotive sector, and battery electric vehicles (BEVs) and hybrid electric vehicles (HEVs) are being vehemently developed as the environmentally friendly alternative to conventional combustion engine vehicles.

Automotive companies have developed multiple vehicles in the recent years to fuel the public's need for alternative forms of transport, with major automotive companies such as Ford, Nissan, Chevrolet, and BMW releasing electric vehicles (EVs) [25]. The outlook for the future of the electric vehicle is positive, with major financial incentives for researchers and automotive manufacturers from the United States Administration, famously pushing for one million EVs on the road by 2015 [23]. This ambitious goal, coupled with recent advances in battery technology, has sparked the emergence and gain in popularity of several specialized BEV companies such as Tesla Motors, whose Model S electric car has a wait time of up to three months [20].

The sales of BEVs and HEVs are not at the level of that of their gasoline powered counterparts despite the growing public interest. Total BEV sales in 2012 total to 14,600 units in the United States, which pales in comparison to the 316,000 vehicles of the same class sold by Ford Motor Company alone [55, 78]. Relatively low penetration of EVs into

the automotive market has been due to two main reasons: 'range anxiety', or a fear of the lack of range EVs have due to a limited size battery pack, and the varying mileage and performance of the EVs during and after operation in extreme ambient conditions.

FleetCarma has explored the effect of vehicle operation in various ambient conditions on the Nissan Leaf, gathering data from real world drivers on more than 5,400 individual trips. They found a drastic decrease in total available mileage in cold weather operation, with drivers reporting an average range of 60km from a fully charged battery during vehicle operation at -25°C, compared to an average range of 106km when operating at 30°C [39]. Conversely, for operation in higher environment temperatures, independent tests performed by Nissan Leaf owners in Arizona have shown a permanent 15% loss in capacity after operation for one summer[30]. These real world user generated results highlight the importance of understanding and quantifying the effects of operating temperature on battery characteristics, and the need for a well designed thermal management system for EVs due the short and long term effects that extreme environmental temperatures have on the EV performance.

The performance of EVs and HEVs depends on the performance of their battery packs. Batteries are electrochemical devices, hence their performance is greatly affected by temperature. To realize the importance of temperature control on the battery, the effects of temperature on the battery must be quantified. The detrimental effects of temperature on the battery pack can be avoided through the use of an effective thermal management system which can keep the battery at an optimum temperature during operation. The design of such a system requires accurate knowledge of the heat generation of the battery at all the operating and discharge conditions experienced by EVs and HEVs.

1.1 Lithium Ion Batteries

A battery is an energy storage device. The most common battery chemistry on the market today for use in automotive applications is the Lithium ion battery (Li-ion), due to its superior power density and minimal memory effects [7, 17]. Li-ion is also the only battery chemistry that will be expected to attain a specific power level of 400W/kg in the near

Table 1.1: Advantages and Disadvantages of Li-ion Batteries [67]

Advantages
High energy density and specific energy
Long cycle life
Low self discharge rate
No memory effect
High open circuit voltage (approximately 4V)
Disadvantages
Potential safety problems due to explosions, fires, caused by thermal runaway
Relatively poor low-temperature performance
Degradation of battery chemistry at high temperatures

future [29]. The main advantages and disadvantages to Li-ion batteries are summarized in Table 1.1.

Different battery components can provide various benefits for the overall battery system. Desired characteristics that can be adjusted through the use of various battery components include non-toxicity, decreased degradation at higher temperatures, and higher power to weight ratio. The main components of a Li-ion battery system and their effects on battery characteristics will be examined in the next section.

1.1.1 Lithium Ion Battery Components

A battery is composed of numerous cells, each of which consists of four major components [67]:

1. Anode, or negative electrode, which gives up electrons to the external circuit; the anode is oxidized during the electrochemical reaction.

2. Cathode, or positive electrode, which accepts electrons from the external circuit; the cathode is reduced during the electrochemical reaction.

3. Electrolyte, or ionic conductor, which is the medium for the transfer of charge or ions in the external circuit. The electrolyte is typically a liquid, containing salts, acids, or alkalis to increases its ionic conductivity.

4. Separators, a micro-porous layer which electrically isolate the positive and electrodes to prevent short circuiting during the electrochemical reaction.

The selection of battery components is integral to the capabilities of the Li-ion cell. The components of the cell have to be chosen to increase the power to weight ratio of the battery, and to increase cell voltage and capacity. The anode needs to be efficient as a reducing agent, have a high coulombic output, and have high electrical conductivity [67]. Carbon based electrodes are commonly used due to their stable surface morphology, which results in consistent safety properties throughout the battery lifetime [65].

For the cathode, the selected material must be an effective oxidizing agent, be chemically stable while in contact with the electrolytic material, be able to incorporate large quantities of lithium without structural change, and have high lithium ion diffusivity [67]. Cathodic materials are commonly made of oxides of transition metals. The performance of cathodes depend on their micro-structure, since the exchange of lithium ions with the electrolyte during charge and discharge occurs at the electrode-electrolyte interface [84]. Recently, a great amount of attention has gone into the development of nano-structured electrodes (such as the $LiFePO_4$ cathode) with increased surface and inter-facial areas which improves electrolyte contact at the electrode interface, hence improving the overall performance of the cell [9, 14, 52].

The electrolyte must be made of materials that have high ionic conductivity. Low toxicity, thermal stability, and low reactivity with other cell components are among the essential characteristics of the electrolyte [67]. The most commonly used electrolyte is formulated with carbonate solvents which are aprotic, polar, and have a high dielectric constant. Electrolytes can be specialized to low temperature applications by using low viscosity solutions with low freezing points [67].

Separators are typically micro-porous films about 16μm to 40μm thick, made of polyolefin materials, due to their mechanical properties, chemical stability, and low cost [67]. Desired mechanical properties of the battery separator include high material strength to

allow automated winding during production of the battery, high resistance to perforations, high wettability by the electrolyte, and compatibility and stability with electrolyte and electrode materials [22]. Currently, separators consist of polyethylene or polypropylene materials which can act as a safety component due to the melting point of the polymer at 135°C an d 155°C respectively. As the inner temperature of the battery reaches the melting points of the polymers, the pores in the separators close and stop the transport of Li^+ ions from the electrodes, thus stopping the battery from discharging or charging further and avoiding potential thermal runaway scenarios [67].

For this thesis, the battery chemistry used in all the experimentation is a prismatic $LiFePO_4$ 20Ah battery from A123 Systems (A123M1HD-A) [36]. The $LiFePO_4$ battery is unique because it uses nano-structured electrodes to increase lithium ion transport in order to facilitate high discharge rates, instead of an electrode with high electronic conductivity and lithium ion transport mobility like the conventional Li-ion chemistries [36]. The $LiFePO_4$ battery chemistry is very safe due to its non-reactive nature with electrolytes in both charged or discharged state at high temperatures, making it an ideal candidate for automotive applications [67].

1.1.2 Electrochemical Mechanisms of the Lithium Ion Battery

During the charging and discharging process of a Li-ion battery, lithium ions are inserted or extracted from the interstitial space between the atomic layers within the conductive materials. The movement of ions and electrons in a typical Li-ion cell is shown in Figure 1.1. The electrochemical reactions of the $LiFePO_4$ cell can be characterized as follows [32],

$$\begin{aligned} \text{Positive reaction} \quad & Li_{1-x}FePO_4 + xLi^+ + xe^- \rightleftharpoons LiFePO_4 \\ \text{Negative reaction} \quad & Li_xC_6 \rightleftharpoons C_6 + xLi^+ + xe^- \\ \text{Total reaction} \quad & Li_{1-x}FePO_4 + Li_xC_6 \rightleftharpoons LiFePO_4 + C_6 \end{aligned} \tag{1.1}$$

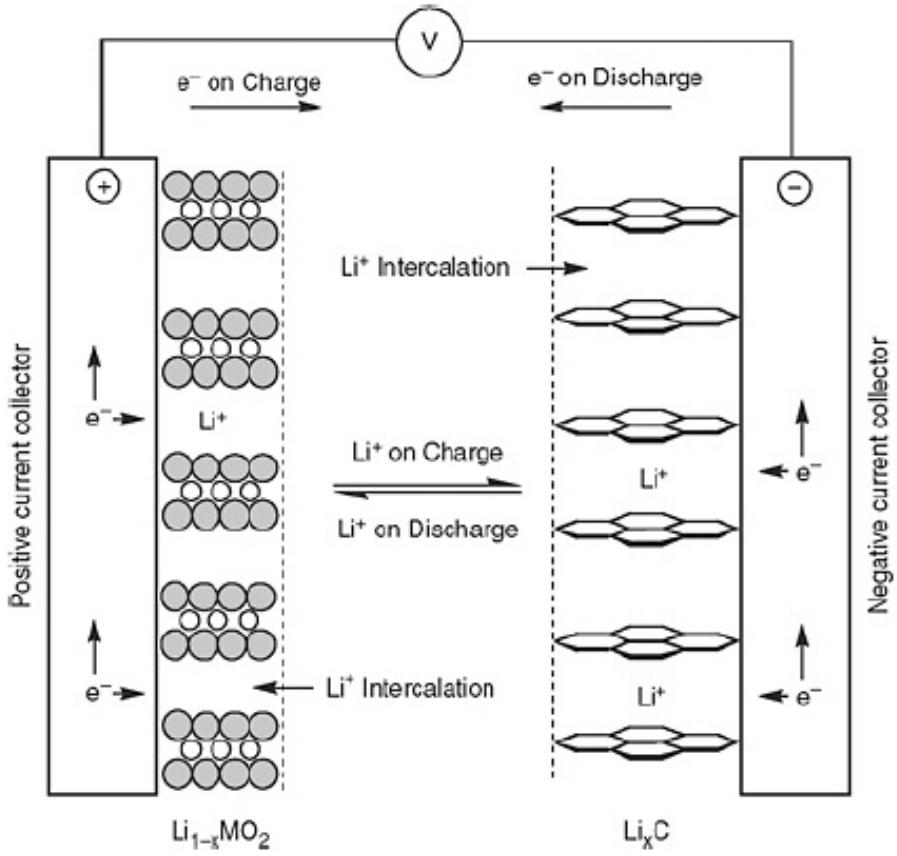

Figure 1.1: Schematic of the electrochemical processes in a Li-ion cell [67]

The reactions proceed from the left side to the right side during the discharge and in the reverse direction during the charge cycle. The maximum electric energy that can be extracted from any electrochemical cell depends on the change in Gibbs energy of the overall reaction in the cell, ΔG [67],

$$\Delta G^\circ = -nFE^\circ \tag{1.2}$$

where F is the Faraday constant, E° is the electromotive force, and n is the number of electrons that flow through the circuit. The maximum theoretical energy cannot be achieved by a real cell however, due to the losses that occur in the cell due to current

flow. These losses can be classified mainly into activation polarization, concentration polarization, and ohmic polarization.

Activation polarization drives the electrochemical reaction at the surfaces of the cathode and anode [67]. Concentration gradients are formed at the interface between the electrolyte and the electrode materials due to the natural resistance to mass transport in the cell [76]. Ohmic polarization, commonly referred to as IR drop in potential, is due to current flow through the internal resistance of the battery [67]. The cell voltage due to effects of the overpotentials can be calculated from [67],

$$E = E_o - [(\eta_{ap})_a + (\eta_{cp})_a] - [(\eta_{ap})_c + (\eta_{cp})_c] - IR \tag{1.3}$$

where E_o [V] is the open circuit voltage of a cell; $(\eta_{ap})_a$ and $(\eta_{ap})_n$ [V] are the activation polarization at the anode and cathode, $(\eta_{cp})_a$ and $(\eta_{cp})_n$ [V] are the concentration polarization at the anode and cathode respectively; I [A] is the current flow of the cell; and R [Ω] is the internal resistance of the cell. The effect of the overpotentials on battery voltage is shown in Figure 1.2. It can be seen that polarization losses from all sources increases as current flow increases, causing a larger deviation of actual cell voltage from open circuit voltage.

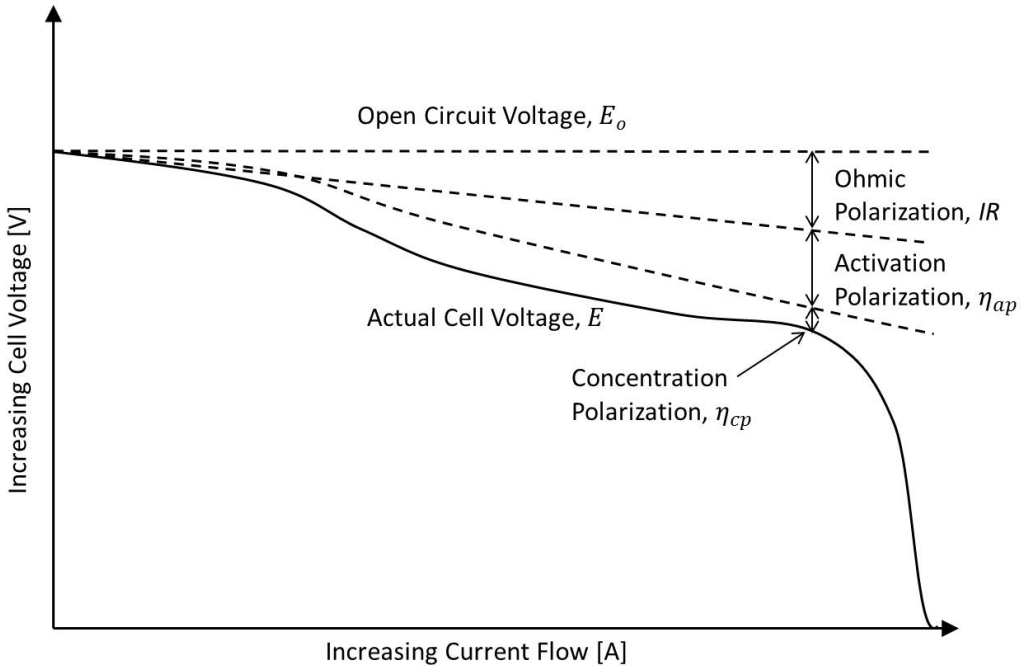

Figure 1.2: Polarization curve of a battery, showing the effect of activation polarization, concentration polarization, and IR drop on open circuit voltage of a cell as a function of cell current [67]

Non-equilibrium effects due to current flow on the electrochemical reaction in the cell are not described in Equation 1.3. The effect of current draw on the on the voltage of the cell has an exponential relation, described by the Tafel equation [67],

$$\eta = a \pm b \log i \tag{1.4}$$

where η is polarization due to current flow within the cell, and a and b are constants.

Polarization of the cell causes the electrical energy to be converted to heat [67]. The exact amounts of heat generation from polarization are hard to quantify, due to the proprietary make-up of the tested battery, and the effects that different battery additives have on the polarization sources. Batteries are electrochemical devices, and therefore temperature also has an effect on the cell open circuit voltage, as well as the polarizations that occur. Low temperature operation causes higher charge transfer resistance, decreased diffusion

rates of salts, and decreased ionic conductivity in the battery, which negatively affect the charging and discharging abilities of the battery [63, 89]. Battery operation at an high temperatures accelerates the electrolyte decomposition and reduces the accessible surface area of electrode particles, which leads to power and capacity fade when high temperature operation is sustained [69, 80]. Therefore, to accurately characterize battery performance, it is imperative to control and observe the effects of both temperature and current draw.

1.1.3 Types of Lithium Ion Batteries

Li-ion batteries are available in multiple forms, most commonly as coin, cylindrical, and prismatic types. The internal structures of the different battery types can be seen in Figure 1.3 [74]. Battery units which are composed of multiple battery cells are linked in series and/or parallel connections to form battery packs to conform to the electrical needs of a particular application, such as a power source for an electric vehicle [57]. The main difference between prismatic and the other types is that the battery electrochemical materials are in layers parallel to each other with central current collectors (anode and cathode), which results in prismatic batteries having a large surface area while being thin. This difference in form offers an advantage in thermal management for prismatic batteries due to a lack of temperature gradient in the thickness of the battery when compared to the Li-ion batteries of other forms.

Coin and cylindrical types are most commonly used in consumer electronics, and have been the subject of the earlier works in the battery electrochemical field. Prismatic Li-ion batteries have emerged recently as the form of choice for applications in the automotive industry due to their higher energy content and high packing factor, and operate on the same principles as the other types.

1.2 Motivation For This Work

The negative effects of operating temperature on battery performance are major concerns with using Li-ion batteries as a form of energy storage device for vehicles; battery capacity

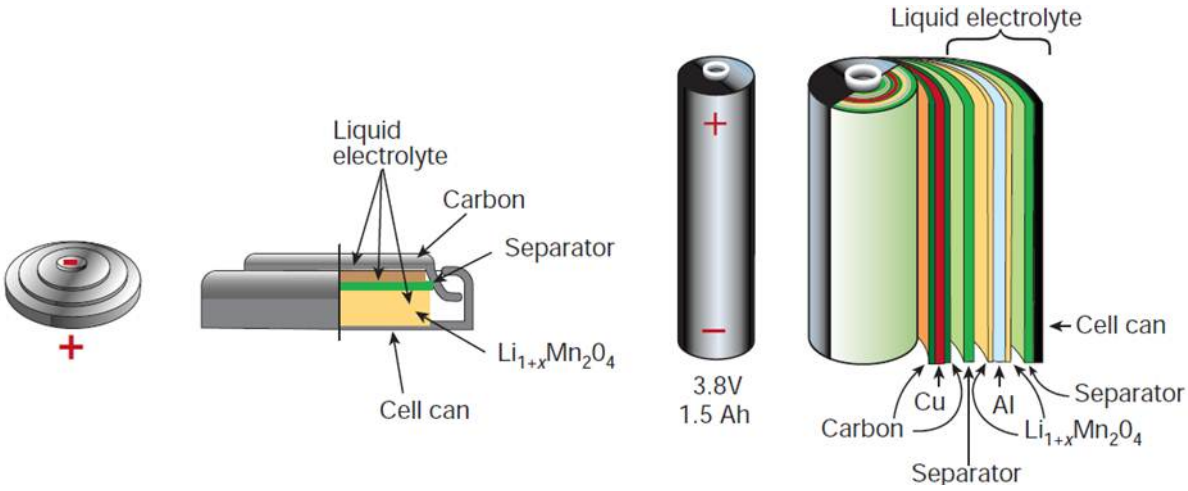

(a) Coin Battery

(b) Cylindrical Battery

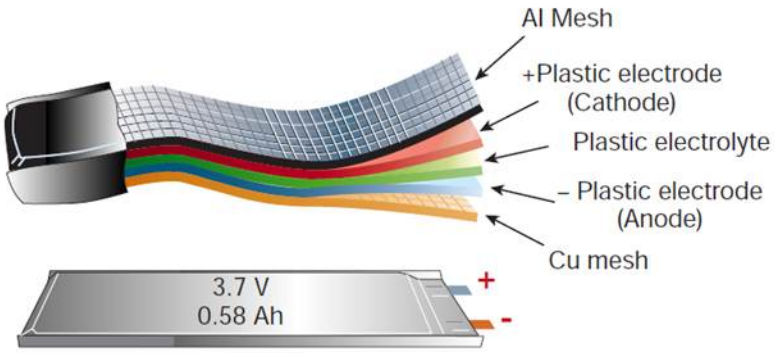

(c) Prismatic Battery

Figure 1.3: A comparison of the internal setup of coin, cylindrical, and prismatic batteries [74]

is decreased at low operating temperatures, and battery degradation increases during sustained operating at high temperatures. The broad effect of temperature on electrochemical devices are well known, but the detrimental effects of temperature on prismatic batteries need to be quantified to highlight the importance of an effective thermal management system. In order to characterize the effect of temperature accurately, a method of battery temperature control needs to be developed such that battery temperature can be kept at isothermal conditions regardless of discharge rate or internal heat generation.

Quantification of the effects of temperature on battery characteristics highlights the importance of developing an effective thermal management system that is capable of keeping the batteries at an optimum operating temperature. The design of such a system requires precise knowledge of the heat generation rates of Li-ion battery at varying operating temperatures and discharge conditions. Modelling the heat generation of the batteries is difficult, due to the complexities in the heat generation and electrochemical mechanisms. Hence, an experimental facility needs to be developed to accurately characterize the heat generation rates of the battery at various discharge and operating conditions to examine the effects of operating temperature and discharge rate on the overall heat generation characteristics of the battery.

1.3 Scope and Outline of This Thesis

In this thesis, experimental facilities are developed to aid in both the accurate quantification of temperature effects on Li-ion battery performance, and the measurement of Li-ion battery heat generation at various discharge rates and operating conditions. The developed experimental techniques are applicable to large prismatic batteries, regardless of battery chemistries. The tested battery in this thesis is a commercially available 20Ah $LiFePO_4$ battery from A123, which is used in automotive applications. The results presented in this thesis are of interest to both the research community and industry, providing benchmark data for comparison to simulation results, as well as battery heat generation characteristics to aid in the design of an effective thermal management system.

This thesis is divided into five chapters. In chapter one, the physical components of batteries are highlighted, the electrochemical mechanisms behind Li-ion batteries are ex-

plored, and the differences and similarities between Li-ion batteries of different forms are discussed. In chapter two, a new experimental technique that allows accurate battery characterization at various operating conditions and discharge rates through precise temperature control of the battery is developed, and the effect of operating temperature on battery performance is quantified through experimentation. In chapter three, a literature review of techniques used in experimental measurements of heat generation rates of various Li-ion batteries is presented, an experimental apparatus is developed to accurately measure the heat generation rates of prismatic Li-ion batteries, and the data reduction technique and equipment calibration will be discussed. Chapter four discusses the results of the measurement, concentrating on the underlying heat generation mechanisms of the battery. Finally, chapter five summarizes the major conclusions and presents recommendations for future work.

Chapter 2

Quantifying Temperature Effects on the Performance of Lithium Ion Batteries

2.1 Literature Review

Battery powered vehicles will operate in a multitude of conditions, from high temperature conditions in the summer to low temperature conditions in the winter, and these temperature changes will strongly influence the performance, driving range, and durability of BEVs and HEVs. Hence, it is very important to investigate the effect of operating temperature on battery discharge characteristics, both to increase the accuracy of state-of-charge (SOC) determination for BEV and HEV drivers, and to develop effective thermal management systems to prolong the lifetime and output capabilities of the Li-ion battery systems.

A common method used in battery analysis is to use experimentally determined coefficients and electrochemical equations based on battery open circuit voltage, internal resistance, discharge current, and state of charge. This technique is based on the work of Shepherd [70], expanded by Tremblay and Dessaint [77], which is currently being used by Simulink for electric vehicle modelling. Due to the nature of the experimentally determined constants and the strong dependence of battery characteristics on temperature,

spatial and temporal temperature control of the battery is extremely important during battery characterization tests, both of which could be challenging. Temporal temperature control requires extracting the amount of heat generated internally by the battery, which is a function of both temperature and SOC of the battery. Spatial temperature control is difficult due to the typical dimensions of the prismatic Li-ion battery (20cm x 16cm x 0.7cm for this study). The order of magnitude difference between the thickness and the other dimensions in the prismatic battery design lends itself to the edge collection of current, leading to high temperatures near the current collection point due to joule heating. The work of Tremblay and Dessaint did not specify the test procedure for the validation of their model, only that it was compared to discharge curves provided by the manufacturer [77]. It might be assumed that discharge in air convection environmental chamber is used, as it is common practice by manufacturers to test batteries in that fashion.

Li-ion battery charging and discharging characteristics are strongly dependent on its operating temperature. Zhang et al. found the performance of the Li-ion battery is affected by the charge-transfer resistance of the battery, which increases exponentially at sub-zero temperatures when compared to operation at a reference temperature of 20°C, decreasing the charging and discharging characteristics of the battery [89]. Choi and Lim demonstrated that the electrical performance of 18650 Li-ion batteries depends significantly on the operating temperature, with a decrease of approximately 95% in energy density for the batteries at -40°C when compared to the same discharge rate at 20°C [19]. Andre et al. showed a strong dependence of electrolyte (or ohmic) resistance and solid electrolyte interface resistance on battery temperature, both of which affect charge transfer and ion diffusion resistance [4]. Pals and Newman found a strong correlation between battery temperature and performance, with an increase in battery performance due to higher diffusion rate of salts and increased ionic conductivity at higher battery temperatures [63]. Both Thomas et al. and Reynier et al. established the existence of a linear dependence of battery open circuit potential with battery temperatures between 20°C and 29°C [68, 76].

Spatial control of Li-ion battery temperature is also extremely important for the accuracy of battery characterization testing. Fleckenstein et al found the cause of divergence of the local SOC and electric inhomogeneities to be due to spatial temperature gradients within the battery [28]. Various studies have shown large spatial temperature gradient

within the battery at the end of discharge due to varying current distributions within the battery [6, 41, 46].

Simulations and experimental studies have been conducted to investigate the effect of heat generation on the spatial temperature distribution in the battery, and results show local temperature of the battery is the highest at the positive and negative terminals of the batteries at the end of discharge due to the higher current density at these locations [6, 41, 46]. For example, a maximum spatial temperature variation of 10°C is shown to occur at a high discharge rate of 5C [44]. Spatial temperature variation in the battery can cause SOC drift and variations in current densities due to the temperature dependence of both the ratio of charge to discharge pulse impedance and open circuit potential [28]. A summary of the results of these studies is shown in Table 2.1.

Table 2.1: Spatial temperature variation of Li-ion batteries at various discharge rates at the end of the discharge process

Author	Battery Used	Rate of Discharge	Spatial Temperature Variation at End of Discharge	
			Low	High
Jeon et al [41]	2Ah 18650 Cylindrical Li-ion Cell	1C	36°C	40°C
Awarke et al [6]	40Ah KOKAM SLPB10021621H Prismatic Li-ion Cell	4C	26°C	37°C
Kim et al [44]	10Ah VLK07 Prismatic Li-ion Cell	5C	48°C	58°C

Various authors have tried to determine the discharge and charge capabilities of a variety of battery chemistries to increase accuracy in SOC estimation and characterize battery performance at various temperatures [3, 6, 16, 34, 42, 60]. These studies employ multiple methods of temperature control for the tests, using a variety of commercially available convective air cooling chambers which are not effective for battery temperature

control due to the low specific heat value of air. To achieve effective temperature control removing the heat generated in the battery, a large flow rate of air needs to be circulated within the chamber, which is not usually done due to the inability of the chamber to increase flow rate. In reality, this can cause large local temperature gradients within the batteries, and hence is not commonly practised. Custom-built conduction chambers also lack the ability to keep the battery isothermal due to the inability of the construction material to conduct out the heat generated by the battery, especially at higher battery heat generation rates occurring at high rates of discharge [3, 34]. Various experimental methods and the temperature increase of the battery are shown in Table 2.2. It is seen that substantial temperature increase, as large as 30°C temporally, has been observed in literature when using the conventional air convection temperature control method at a discharge rate of 2C [16].

Table 2.2: Comparison of various test methods and their respective temporal temperature variations over the entire discharge cycles

Author	Experimental Method	Battery Used	Temperature Variation Over Disharge	
			1C	2C
Hallaj et al [3, 34]	Insulative Conduction Chamber	2Ah 18650 Cylindrical Li-ion Cell	11°C	—
Onda et al [42, 60]	Convective Chamber	2Ah 18650 Cylindrical Li-ion Cell	25°C	—
Awarke et al [6]	Free Convection in Ambience	40Ah KOKAM SLPB10021621H Prismatic Li-ion Cell	—	37°C
Chacko et al [16]	Convective Chamber	Prismatic 20Ah LiNiMnCoO2 Cell	15°C	30°C

From the above literature review, it is apparent that battery temperature control is extremely important, both spatially and temporally. The current battery temperature

control, using a method of air convective cooling either in the form of forced convective cooling, in temperature control chamber or free convection in ambient conditions, is inadequate to ensure the accurate control of battery temperature during discharge. Therefore, the objective of the work in this chapter is to develop a method for the accurate control of the operating temperature of large prismatic batteries throughout discharge process, for the discharge rates and operating temperatures typically encountered in electric vehicles. In this section, a water-ethylene glycol mixture (WEG) in a thermal bath is used for battery temperature control, and a prismatic $LiFePO_4$ battery from A123 is used to exhibit the differences that can be observed in the battery characterization results when using the developed technique versus the conventional method of battery temperature control. It will be shown that this WEG temperature control method is effective at maintaining the battery at isothermal conditions both temporally and spatially and significantly improves the accuracy of battery characterization. A comparison with the conventional air convective temperature control method will be made.

2.2 Experimental Setup

The test method employs a water-ethylene glycol mixture as the coolant for battery temperature control. A mixture of 50-50 water-ethylene glycol is employed, allowing a battery temperature range of -20°C to 100°C. The battery is immersed in a constant temperature bath (ThermoFisher A25B, ±0.1°C) with the terminals held above liquid level. A cover with a thermal resistance value $0.87 m^2 KW^{-1}$ measuring 0.23m by 0.25m and a thickness of 0.005m is fitted over the batteries to decrease evaporation from the bath, and to prevent heat loss from the bath to the ambient. The fluid mixture is agitated around the battery through the use of the built-in agitator pump, creating a significant flow of the coolant past the battery surface, providing enhanced heat transfer. The heat gained by the cooling fluid via heat transfer from the battery is removed using a refrigeration coil built into the bath. The experimental setup is shown in Figure 3.1.

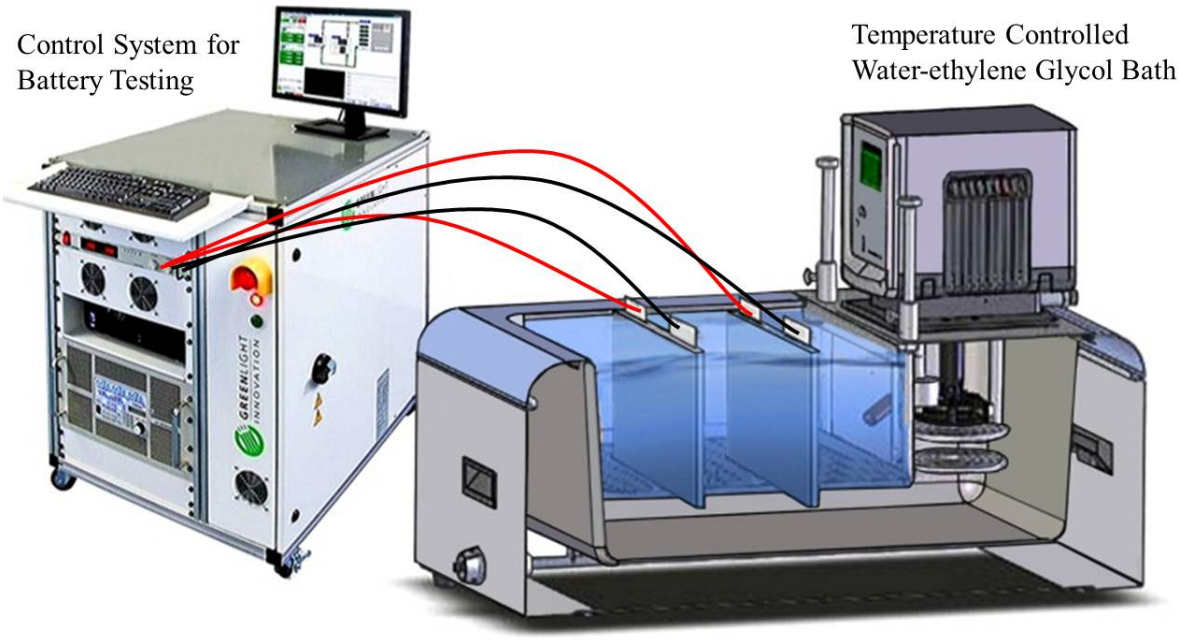

Figure 2.1: Experimental setup for water-ethylene glycol (WEG) temperature control method

Discharge tests are performed on a commercially available prismatic Li-ion battery ($LiFePO_4$) from A123, with a nominal capacity of 20Ah (A123M1HD-A). To normalize the results for comparison purposes, discharge rates will be given in C-rates, where 1C is the discharge rate at which the battery will be fully depleted in an hour (20A), 2C is the discharge rate at which the battery will be fully depleted in 30min (40A), etc. Surface temperature of the battery at 8 different locations on each face of the battery as shown in Figure 2.2 is recorded using high accuracy thermocouple (accuracy $\pm$ 0.1°C). The test battery is cycled through 5 different discharge rates (0.2C, 0.5C, 1C, 2C, 3C) at a six different operating temperatures (-10°C, 0°C, 10°C, 20°C, 30°C, 40°C) from an open circuit voltage of 3.6V to a cutoff voltage of 2.6V. A Greenlight Innovations G12-200 battery test station is used to control the discharge and charge of batteries, which has an accuracy of $\pm$ 0.2A in current source control, $\pm$ 0.05V in voltage source control, $\pm$0.06% full scale in current sink control, and $\pm$0.10% full scale in current measurement.

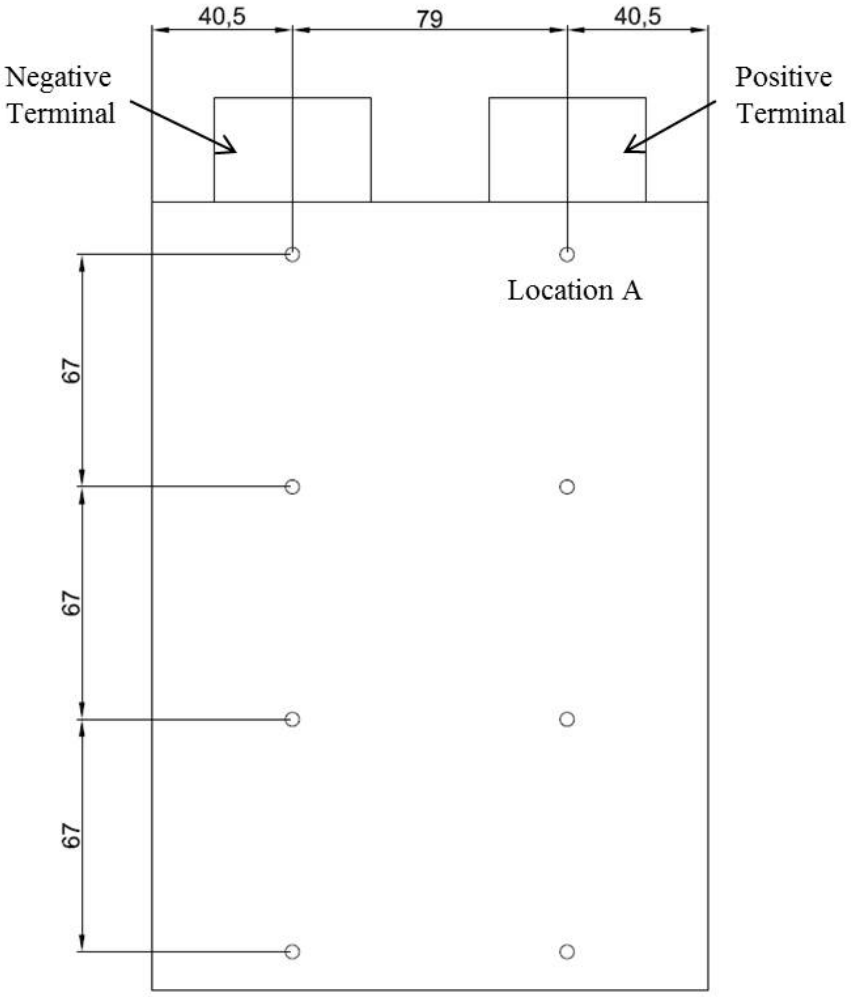

Figure 2.2: Thermocouple locations for battery temperature measurements (all measurements in mm). A total of 16 thermocouples were used, with 8 at corresponding locations on each side of the battery

As a comparison, the conventional air convection temperature control method is also tested using a Cincinnati Sub Zero BZ1 series environmental chamber as shown in Figure 2.3. The battery is shielded from forced convection using a custom-built cover to avoid local hot spots caused by blowing air, and conduction to the chamber is avoided by mounting the test batteries on top of low thermal conductivity stands made of 2mm diameter wooden

dowels, which only contact the battery on four corners. Both the battery cycling and temperature measurements are performed as described earlier.

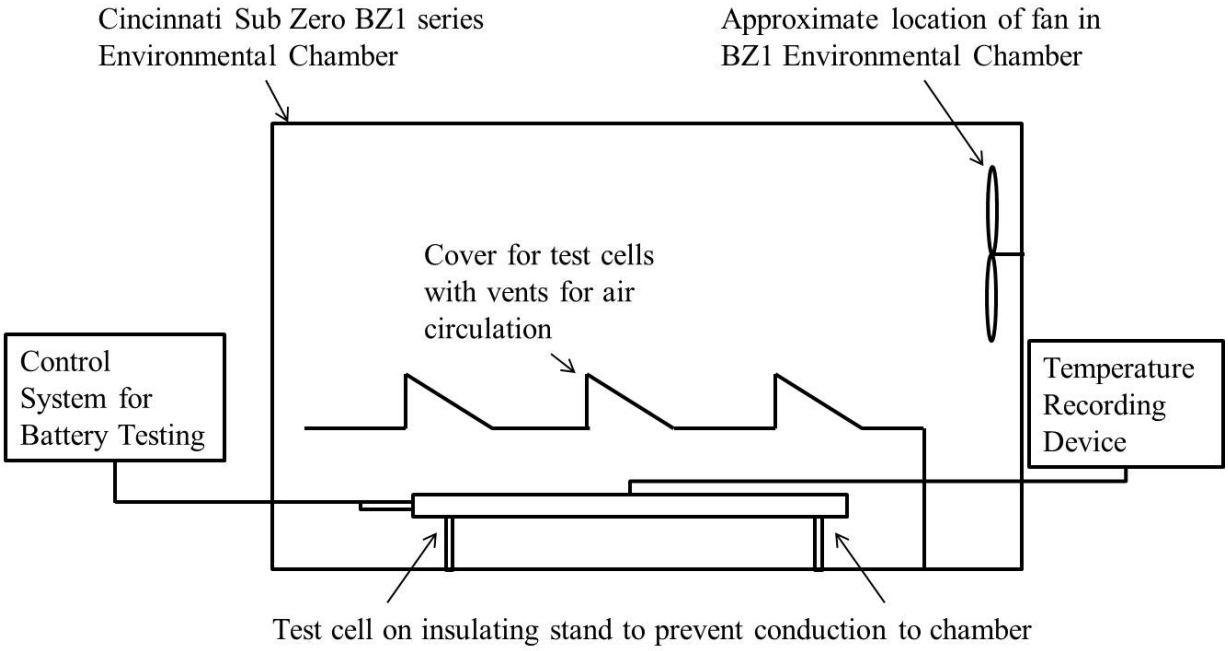

Figure 2.3: Schematic of the conventional air convection temperature control method test setup

The batteries are discharged to cutoff voltage five times for conditioning purposes before testing, which allow irreversible capacity fade which is present in some unused Li-ion batteries to occur [34]. The batteries are brought to the test temperature by the thermal bath, and discharge testing is commenced after the batteries have reached the specified temperature for one hour. The tests are performed in semi-random order, such that no two subsequent discharge tests have the same operating conditions (both temperature and discharge rate) to ensure no condition from the previous test skews the results for the ensuing test. Charging of the battery at C/5 rate is started after a two-hour relaxation period, which allows the battery chemistry to come to equilibrium. Charging of the batteries follows the standard constant current to constant voltage charging scheme. The next discharge cycle commences one hour after the batteries have attained the necessary

temperature. The test schedule is shown in Figure 2.4.

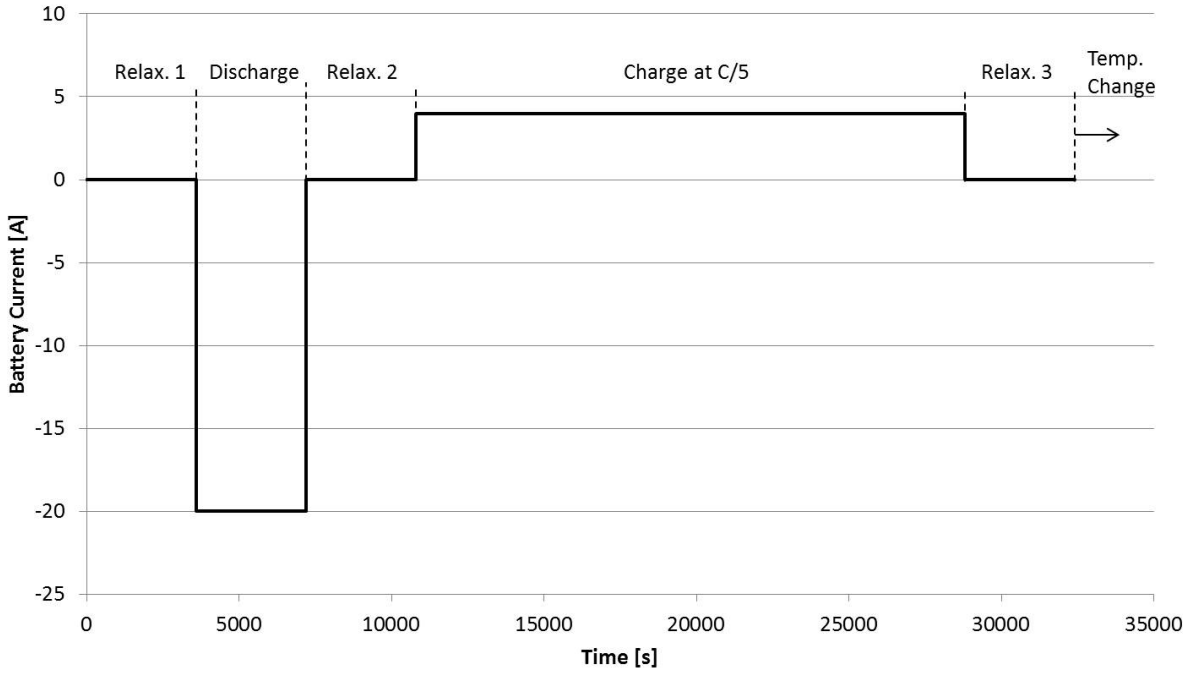

Figure 2.4: Test schedule used in the present study for Li-ion batteries at various discharge rates and operating temperatures

2.3 Comparison of Battery Temperature Control Methods

All battery characterization results shown in this and the subsequent sections are for a single battery, averaged over 5 tests, in order to minimize capacity fade due to battery cycling. Average battery temperatures are calculated using the average of 16 thermocouple readings, and standard deviation, calculated for the average battery temperature over the 5 tests, are in the same order of magnitude as the thermocouple error for all discharge rates for both methods of temperature control. This represents good repeatability in the obtained experimental results.

Figure 2.5 shows that the maximum variation of temporal battery temperature for the conventional air convection method of temperature control is approximately 13.1°C, 11.2°C, and 7.2°C for the 3C, 2C, and 1C discharge rate, respectively. These values can be compared to an increase of less than 0.3°C, 0.2°C, and 0.2°C for the 3C, 2C, and 1C discharge rates, obtained using the WEG temperature control method. The average increase in battery temperature across all 16 locations for the conventional air convection method of temperature control is shown to be in the same order of magnitude as literature, and is orders of magnitudes higher than the results obtained using the WEG temperature control method.

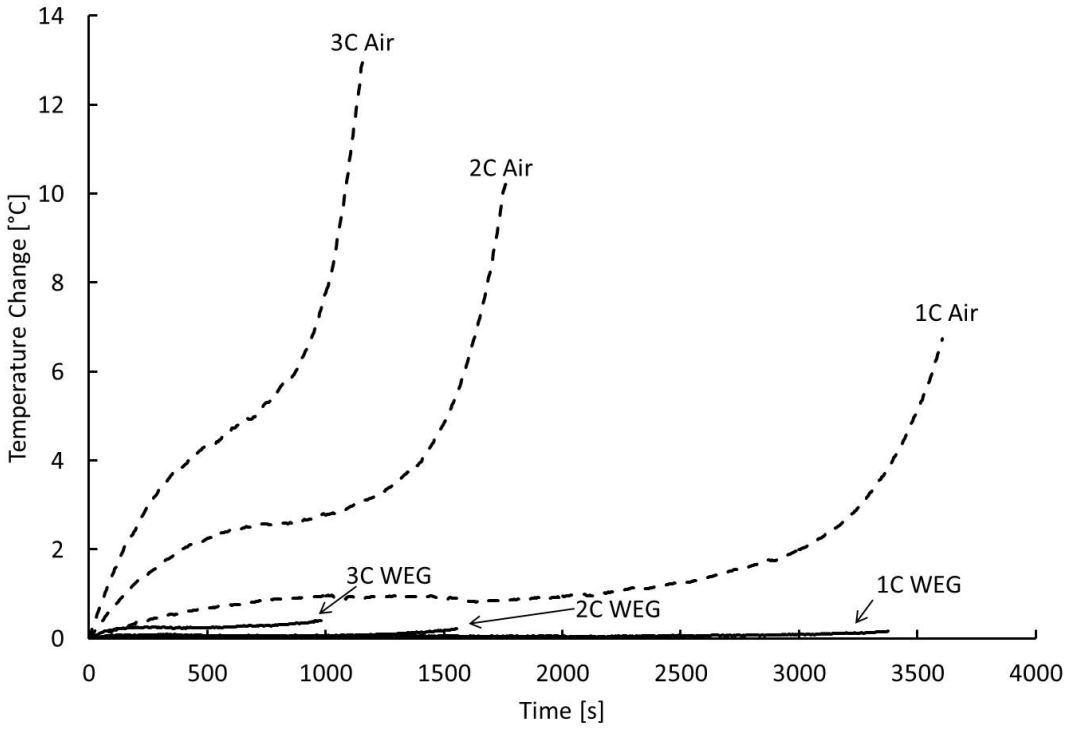

Figure 2.5: Comparison of the increase in battery temperature when discharging at 20°C using the conventional air convection (Air) temperature control method (the dashed curves) and the water-ethylene glycol (WEG) temperature control method (the solid curves) at 1C, 2C, and 3C discharge rate.

The standard deviations of the temperature across the 16 thermocouple locations are shown in Figure 2.6 as a function of time for the 1C discharge rate and the initial battery temperature of 20°C, for both methods of battery temperature control. The standard deviation values are calculated using the average temperature at each thermocouple location over 5 tests. This value can be used as a measure of the spatial temperature gradient in the battery, with larger values signifying a higher deviation from the average battery temperature. The rapid increase in the standard deviation value for air convection temperature control at the end of battery discharge is due to the rapid increase in battery internal heat generation near the end of the discharge test, and the ineffectiveness associated with the lower heat removal rates of using air as a cooling media. The standard deviation of temperature on the test battery using the WEG temperature control method is about ± 0.1°C, which is the same as the accuracy of the thermocouples used in the present measurement and it is much lower than using the conventional air convection temperature control method. This indicates the ability of the WEG method to reduce temperature gradients in the battery throughout discharge.

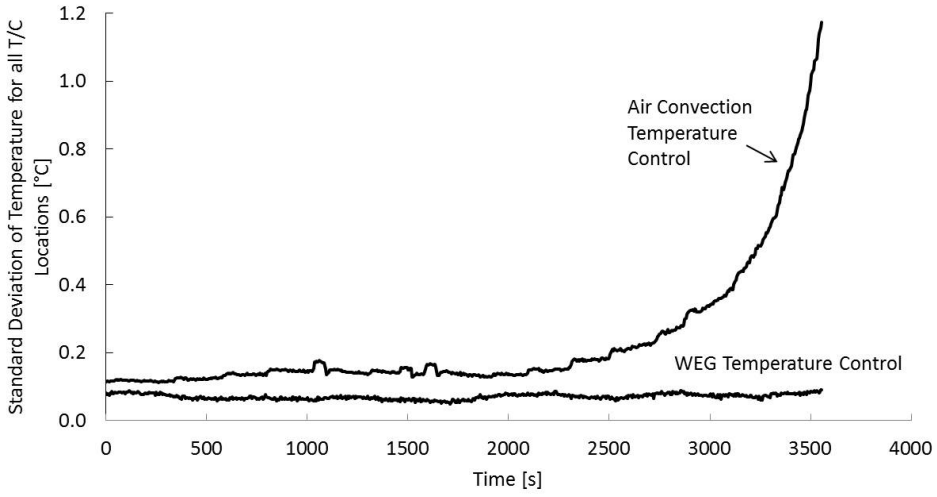

Figure 2.6: Comparison of standard deviations of battery temperature at 16 thermocouple locations (averaged over 5 repetitive tests) between the conventional air convection and water-ethylene glycol (WEG) temperature control method at 1C discharge rate and the set battery temperature of 20°C.

The same Li-ion battery is tested using both the water-ethylene glycol and the conventional air convection temperature control method at 20°C with the discharge rates of 1C, 2C, and 3C to examine the effect of the temperature control on battery discharge characteristics. The results are shown in Figure 2.7. It is seen that a significant difference exists between the battery discharge curves obtained using the two different methods of battery temperature control. In all cases, the measured capacity of the battery is higher when using the conventional air convection temperature control method due to the higher temperature achieved by the battery during the course of testing, as shown in Figure 2.5, with an increase in capacity of 25%, 12%, and 18% for 1C, 2C, and 3C discharge rates, respectively. Although an increase in battery capacity is desired, the results obtained are not representative of the true battery discharge characteristics at the set temperature due to the increase in battery temperature from battery internal heat generation.

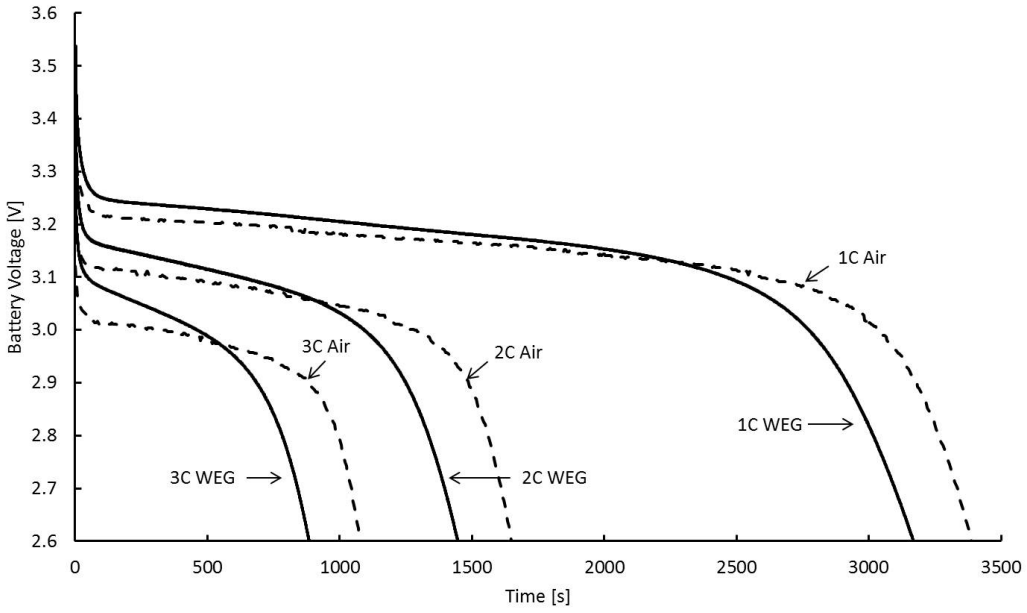

Figure 2.7: Comparison of battery discharge curves when discharging at 20°C using the conventional air convection (Air) temperature control method (the dashed curves) and the water-ethylene glycol (WEG) temperature control method (the solid curves) at 1C, 2C, and 3C discharge rate.

A summary of spatial and temporal temperature variation at 20°C and various discharge rates is shown in Table 2.3. The average temporal temperature variation is calculated by taking the difference in average battery temperature at the beginning and end of the discharge cycle. It is seen that at high rates of discharge (3C, 2C), the average temporal temperature difference is orders of magnitudes higher when the conventional air convection method of temperature control is used. At discharge rates lower than 1C, the results show that the average temporal temperature variation in the battery is the same as the thermocouple error when the WEG temperature control method is employed, essentially maintaining the battery at isothermal conditions temporally. The spatial temperature variation is calculated by taking the standard deviations between the average temperatures at each thermocouple location over 5 tests at the end of discharge, when the spatial temperature variation throughout the battery is the highest. It can be seen that the spatial temperature variations when using the WEG temperature control method is consistently orders of magnitudes lower than the results obtained from using the conventional air convection temperature control method. The results show that the location at which the battery temperature is the highest is always kept to within 0.4°C of the average battery temperature for the WEG method of temperature control, whereas the conventional air convection temperature control method shows a maximum spatial temperature deviation of 4.3°C from the average battery temperature. It can be seen that the spatial temperature variation is kept to below 0.4°C for all discharge conditions tested when using the WEG temperature control method, and shows the ability of the WEG temperature control method to keep spatial temperature variation to a minimum compared to using the conventional air convection method of temperature control.

Table 2.3: Summary of test results for batteries at 20°C and various discharge rates, outlining the average temporal and spatial temperature variation for the discharge tests for both the water-ethylene glycol (WEG) and conventional air convection (air) temperature control methods

Discharge Condition	Average Temporal Temperature Variation		Maximum Spatial TemperatureVariation	
	WEG (°C)	Air (°C)	WEG (°C)	Air (°C)
3C	0.3	13.1	0.4	4.3
2C	0.2	11.2	0.2	2.1
1C	0.2	7.2	0.1	1.2
0.5C	0.1	5.5	0.1	1.0
0.25C	0.1	4.5	0.1	1.0

The presented results show a clear advantage of using the WEG temperature control method due to its ability to control the battery at near isothermal conditions temporally in spite of the internal heat generation of the battery, and the drastic decrease of spatial temperature deviation throughout the discharge tests, potentially eliminating SOC drift and varying current density within the battery.

2.4 Effect of Operating Temperature on Battery Discharge Characteristics

The battery discharge curves for various temperatures at 3C discharge rate, obtained using the water-ethylene glycol temperature control method, is seen in Figure 2.8. Figure 2.8 shows the reduction in battery capacity with lower temperatures, due to the decrease in the ionic conductivity of electrolyte and solid electrolyte interface, and a slowdown of battery electrochemical reactions [89]. Battery capacity decreased by 95% when the battery temperature is lowered from 20°C to -10°C. The optimum operating temperature of the battery is between 20°C and 30°C, where the capacity is near maximum and the

degradation effects due to operation at high temperature is minimized [19]. Increasing the battery temperature to 40°C at a 3C discharge rate increases capacity by 26%, but with the consequence of increased rate of battery degradation. The decrease in battery capacity is sensitive to small changes in temperature; battery testing performed at 22°C and 20°C shows a 2.3% reduction in battery capacity due to the 2°C decrease in battery temperature.

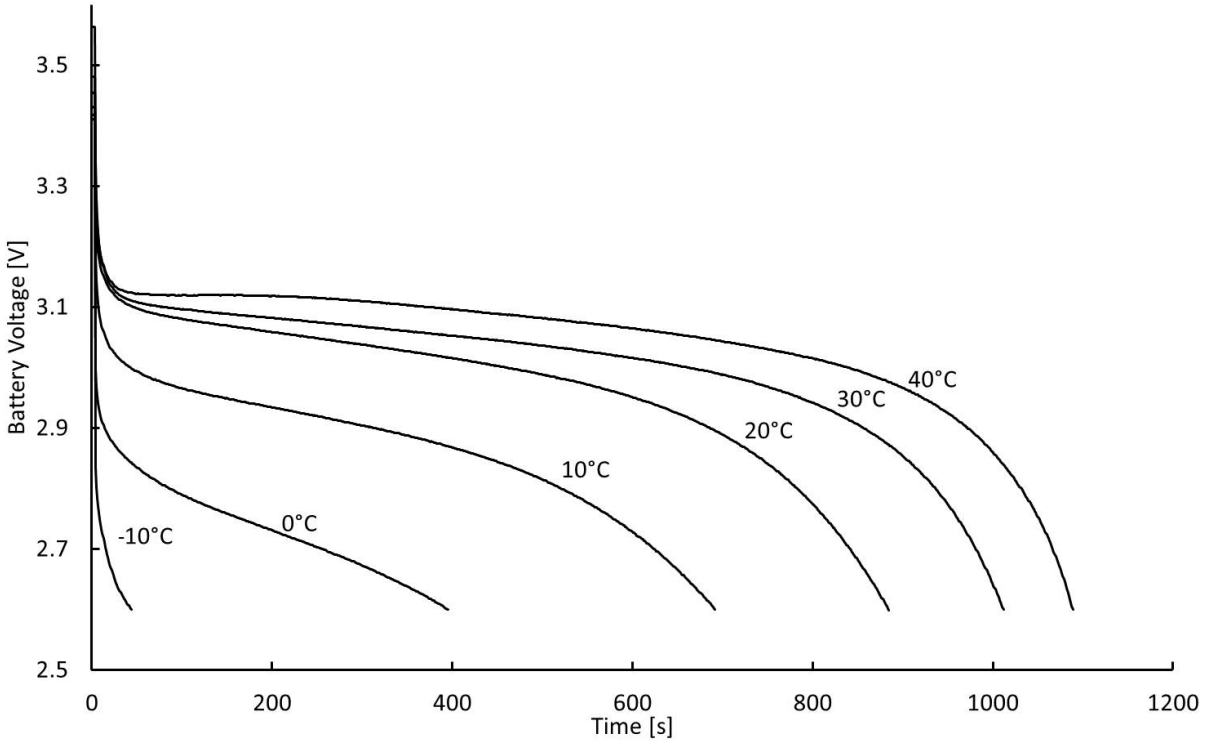

Figure 2.8: Battery discharge curves of the test battery at various temperatures for 3C discharge rate using the water-ethylene glycol temperature control method.

The relationship between battery temperature and battery capacity for all tested operating temperatures and discharge rate can be seen in Figure 2.9. The dramatic decrease in battery capacity at all tested discharge rates due to operation at lower temperatures highlights the importance of an effective thermal management system, especially in colder climates, to keep the batteries at an optimum temperature such that capacity is maximized.

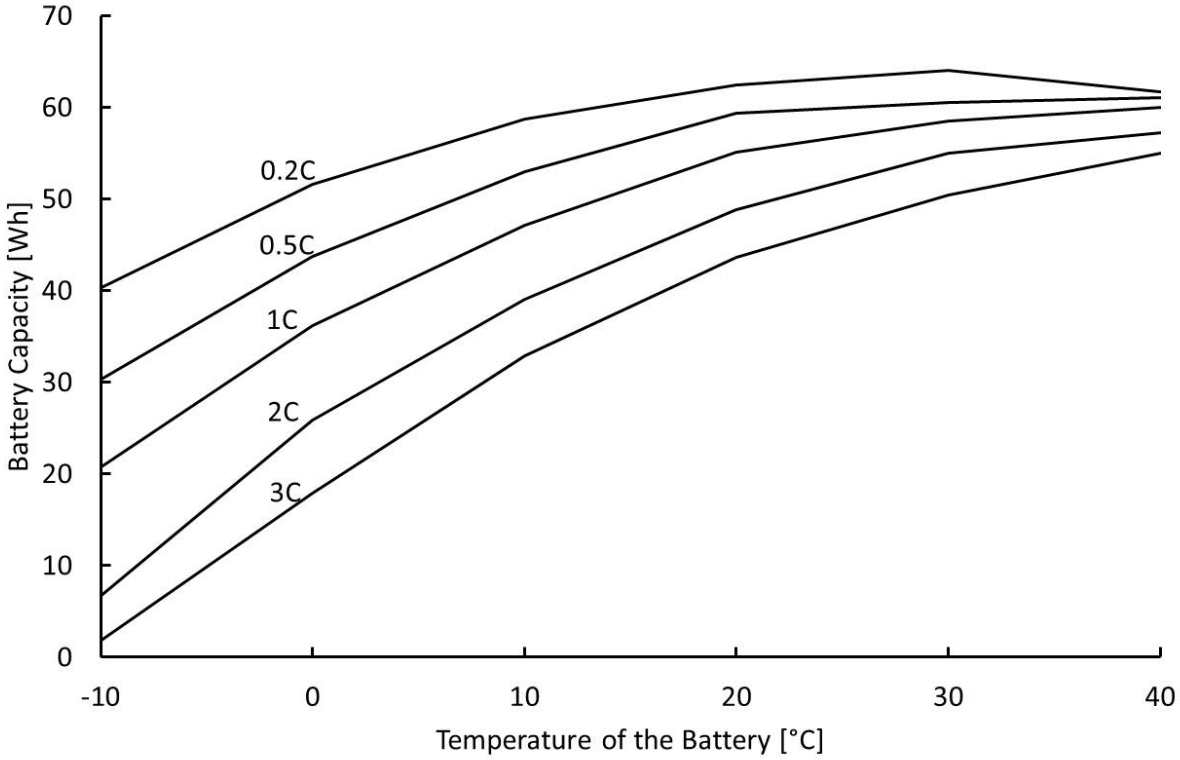

Figure 2.9: Relationship between battery energy and operating temperature for all discharge rates and temperatures tested

Through the observed phenomenon in this experiment, it is seen that conventional methods of using air convection based temperature control chambers are inadequate in keeping the battery at isothermal conditions temporally and spatially. A technique capable of keeping the battery isothermal is developed using a thermal bath, with 50-50 water-ethylene glycol (WEG) solution used as the working fluid in the thermal bath. It is seen that the WEG method of temperature control is much more effective at keeping the battery isothermal, and the differences in battery discharge characteristic due to the temperature control methods are explored. Finally, the effect of battery temperature on the capacity of the battery was examined, and results show drastic decreases in battery capacity when operating at low temperatures for all discharge rates tested. This highlights the importance of developing a thermal management system capable of keeping the battery at an optimum

operating temperature, and hence the need to accurately measure the heat generation rates of the battery under various discharge and operating conditions.

Chapter 3

Calorimetric Measurements of Prismatic Li-ion Batteries

3.1 Literature Review

The work in the previous chapter quantified the detrimental effects of temperature on battery characteristics, and in order to extract to develop a system capable of keeping the battery at isothermal conditions for various operating and discharge conditions, heat generation mechanisms of Li-ion batteries need to be quantified and studied.

Heat generation in Li-ion batteries includes two main components: reversible heat generation due to entropic changes in the battery, and irreversible heat generation due to ohmic losses, charge-transfer overpotentials, and mass transfer limitations [12]. A widely cited expression for the volumetric heat generation rate of the battery, $\dot{q}'''$ (Wm^{-3}), is given as follows [12]

$$\dot{q}''' = i(V_{\mathrm{oc}} - V) - i(T\frac{\partial V_{\mathrm{OC}}}{\partial T}) \tag{3.1}$$

where i (Am^{-3}) is the volumetric current density which is positive for discharge and negative for charge, V_{oc} and V (V) are the open circuit voltage and the instantaneous voltage of the battery respectively, and T (K) is the temperature of the battery.

Higher current densities at the current collectors create additional Joule heating. This additional Joule heating is not an issue for smaller batteries like coin and cylindrical types commonly used in consumer electronics, but is more apparent in batteries of larger form, such as the prismatic type used in EVs and HEVs [31, 46, 47, 86]. An equation describing volumetric heat generation in larger batteries has been developed, accounting for this additional Joule heating due to higher current densities at the current collectors [31, 82],

$$\begin{aligned} \dot{q}''' &= aJ\left[V_{\mathrm{OC}} - V - T\frac{\partial V_{\mathrm{OC}}}{\partial T}\right] + a_p r_p i_p^2 + a_n r_n i_n^2 \\ \vec{i}_{\mathrm{p}} &= -\frac{1}{r_{\mathrm{p}}}\nabla V_{\mathrm{p}} \\ \vec{i}_{\mathrm{n}} &= -\frac{1}{r_{\mathrm{n}}}\nabla V_{\mathrm{n}} \end{aligned} \tag{3.2}$$

where a (m^{-1}) is the specific area of the battery; J (Am^{-2}) is the current density; $\vec{i}_{\mathrm{p}}$ and $\vec{i}_{\mathrm{n}}$ (Am^{-1}) are the current density vectors in the positive and negative electrodes; r_{p} and r_{n} (Ω) are the resistances of the positive and negative electrodes; V_{p} and V_{n} (V) are the potentials of the positive and negative electrodes; a_{p} and a_{n} (m^{-1}) are the specific areas of the positive and negative electrodes, respectively. The addition of the third and fourth terms account for the additional Joule heating of the positive and negative electrodes due to the increased current densities at those sites [31, 82]. The parameters in Equations (3.1) and (3.2) are temperature dependent, and their temperature dependence has to be measured experimentally for specific batteries. These measurements are difficult to perform, owing to the three dimensional distribution of current, the changing electrode resistivity due to current and temperature effects, and the complex behaviour of inter-facial areas of the electrode and electrolyte. Hence, heat generation in a battery is often measured directly.

Heat generation rates of Li-ion batteries are measured with two main methods: accelerated-rate calorimetry (ARC) and isothermal heat conduction calorimetry (IHC), both of which apply a control volume around the battery, and measure the heat generation, $\dot{q}$ [W], such that [7]

$$\dot{q} = MC_p\frac{dT}{dt} + hA(T_{\mathrm{surf}} - T_{\mathrm{sink}}) \tag{3.3}$$

where M (kg) is the mass of the battery, C_p ($\mathrm{Jkg}^{-1}\mathrm{K}^{-1}$) is the heat capacity of the battery, dT/dt (VK^{-1}) is the change in battery temperature with respect to time, hA (WK^{-1}) is

the calorimeter constant, T_{surf} (K) is the surface temperature of the battery, and T_{sink} (K) is the temperature of the thermal sink surrounding the battery.

The ARC method determines the heat generation rate of the battery by measuring the rise in battery temperature over time and the amount of heat expelled from the battery to the surroundings according to Equation (3.3). Li-ion batteries have a layered internal structure, and hence it is difficult to measure its heat capacity accurately. Since the battery is an electrochemical device, changes in the battery temperature during testing could lead to inaccurate heat generation characterization [43]. Hong *et al* used a commercially available accelerated rate calorimeter (ARC2000, Columbia Scientific Industries) to measure the heat generation rates of Sony type US18650 1.35Ah cylindrical Li-ion battery at discharge rates of C/3, C/2, and C/1 at 308K, with the maximum measured heat generation rates of 1.63 WL^{-1} [34]. Al Hallaj *et al* made measurements with the same experimental apparatus on 18650 Li-ion batteries from AT&T and Panasonic, and found maximum heat generation rates of 0.26 WL^{-1} for discharge rates of less than C/10 and charge rates of C/3 [2].

The IHC method utilizes a large heat sink in contact with the surface of the battery to keep the battery at isothermal operation during measurements, hence eliminating the first term in Equation (3.3). This technique confines the measurements to low battery discharge rates, since fast discharge of the battery leads to higher rates of heat generation which the heat sink cannot extract, causing a temperature gradient within the battery [7]. Kim *et al* utilized a commercially available micro-calorimeter (IMC, CSC4400, Calorimetry Science Corp.) to classify the heat generation rates of Li-ion coin type (size 2016) batteries. The heat generation rate of the battery was measured using temperature sensors placed between the battery and an aluminium heat sink and for discharge rates of C/10, C/5, C/3, and C/1 from 300K to 330K. The corresponding maximum heat generation rates were reported as 0.82 WL^{-1} for discharge rates between C/10 and C/5, 0.97 WL^{-1} for discharge rates of C/5 to C/2, and 3.21 WL^{-1} for discharge rates of C/2 to C/1 [45]. Kobayashi *et al* measured the heat generation rates of cylindrical Sony US18650 Li-ion batteries using a Calvet-type conduction micro-calorimeter (MMC5111-U), which has an isothermal aluminium vessel in contact with the test battery, and a thermomodule was used to measure the amount of heat transfer from the battery to the heat sink. The battery was discharged at 1/50C and 1/10C at an ambient temperature of 300K and 330K, and a maximum heat generation

rate of 0.97 WL^{-1} was measured for discharge rates between C/10 and C/5 [50]. Onda *et al* measured the heat generation rates of small cylindrical Sony US18650 Li-ion batteries using a thermal bath as the constant temperature heat sink. The test battery was wrapped in a thin film for electrical insulation, and the temperature of the battery was recorded using a type K thermocouple. The battery was discharged at C/10, C/2, and C/1, with a corresponding maximum measured heat generation rate of 11.0 WL^{-1}, 27.5 WL^{-1}m and 84.5 WL^{-1} [60]. Bang et al used the same equipment as Kim et al to perform in situ heat generation rates of a $LiMn_2O_4$ coin type Li-ion cell. Measurements were performed at discharge rates of C/10, C/7, C/3, and C/1 at battery temperatures between 300K and 330K. The results show a maximum heat generation rate of 0.63 WL^{-1} for discharge rates of C/10 to C/5, 2.65 WL^{-1} for discharge rates of C/5 to C/2, and 7.51 WL^{-1} for discharge rates of C/2 to C/1 [8].

From the above literature review, it is clear that the previous works on the heat generation measurement of Li-ion batteries have exhibited a wide range of results, even for batteries of the same chemistry and form [7]; and they are limited to: (*i*) small sized cylindrical or coin type batteries which are not applicable for HEV and EV use; (*ii*) low rates of discharge ($\leq$C/1) which are not representative of the electrical needs of the EV; (*iii*) battery operation near room temperatures, which do not reflect the wide range of operating temperatures of EVs. Therefore, the objective of the work in this chapter is to measure the heat generation rates for large prismatic type of Li-ion batteries for a wide range of discharge rates and operating temperatures, as encountered by EVs and HEVs. In this chapter, an experimental technique that can accurately measure the heat generation rates of prismatic Li-ion batteries is developed, and the heat generation rates of an A123 prismatic $LiFePO_4$ battery with a 20Ah capacity for use in automotive applications is measured and verified for various discharge and operating conditions.

3.2 Apparatus Design

The calorimeter is constructed by surrounding the battery with a material of known thermal properties (hereafter referred to as calorimeter material) such that a temperature profile within the material can be deduced for any battery heat generation rate. Prismatic

batteries have a high surface area to thickness ratio, which promotes heat transfer from its front and back faces. Hence, the calorimeter is in the form of two identical slabs attached to the front and back faces of the test battery. The heat generated by the battery is conducted through the slabs into a constant temperature heat sink. Measured temperature change within the calorimeter material due to the heat generated by the battery can be used to infer the unknown heat generation rate of the battery. For the calorimeter design process, heat generated by the battery is estimated to be in the range of 10W, and simulations are performed to estimate the temperature rise in the different calorimeter materials of various thickness due to the heat generation rate. High density polyethylene (HDPE) is selected as the calorimeter material due to its stable thermal properties at the planned test temperatures and its high temperature rise due to the estimated heat generation rate of the battery.

An exploded view of the calorimeter is shown in Figure 3.1. The Li-ion battery is placed between two HDPE slabs, both of which are five times the thickness of the battery. A coating of thermal grease is applied to the surface of the battery to minimize contact resistance between the battery and HDPE surfaces. The HDPE slabs with the battery are placed between two aluminium slabs. This prevents deformation of the softer HDPE material during assembly to ensure good surface contact between the battery face and the HDPE. The calorimeter is bolted together in eight locations, tightened in a criss-cross pattern to ensure even tightening, and is immersed in a constant temperature bath (ThermoFisher A25B, accuracy of $\pm 0.1^{\circ}$C). The working fluid within the thermal bath is a 50-50 mixture of water-ethylene glycol, which allows measurements at sub-zero temperatures. Two high accuracy thermocouples (with accuracy of $\pm$ 0.1°C) are embedded 4mm away from the battery contact surface vertically into the HDPE material (one in each slab), centred on the battery. The placement of the thermocouple at the center of the battery minimizes the edge effects of heat transfer from the HDPE to the surroundings. Two additional thermocouples are placed at the surface of the battery to monitor the battery temperature throughout testing (not shown in Figure 3.1). An insulating cover is placed over the assembly such that the battery terminals are exposed to air, which minimizes heat transfer from both the bath and the top of the calorimeter to the ambient. A schematic of the experimental apparatus is shown in Figure 3.2.

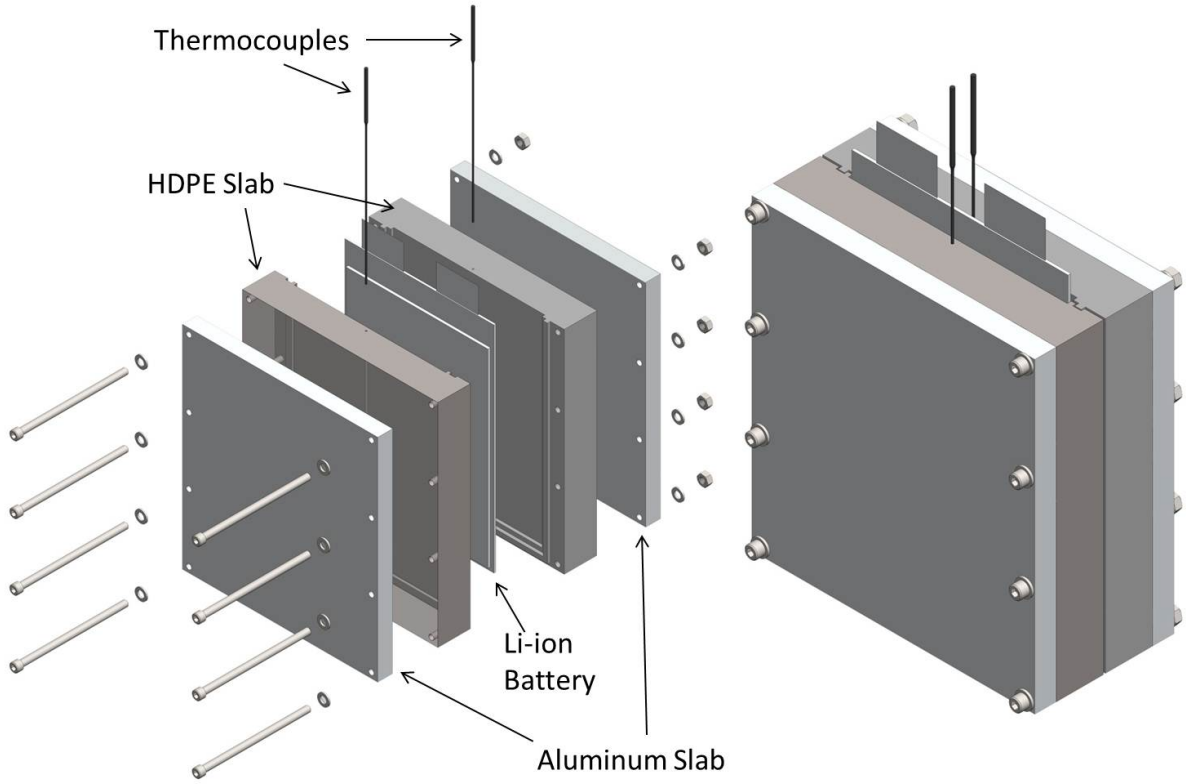

Figure 3.1: Exploded (left) and assembled (right) view of the experimental setup for the measurement of heat generation of prismatic Li-ion batteries. HDPE stands for high density polyethylene.

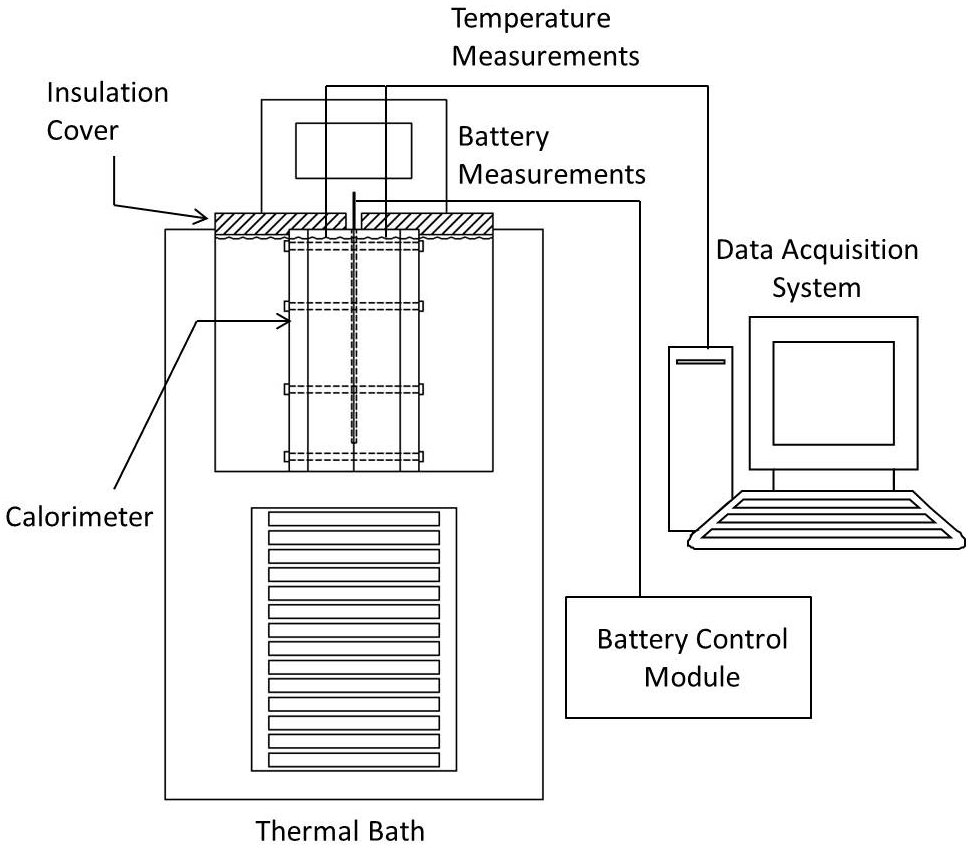

Figure 3.2: Schematic of the complete experimental setup.

The tested battery is the aforementioned $LiFePO_4$ prismatic Li-ion battery from A123, although any battery (Li-ion or otherwise) of prismatic shape can be used in the calorimeter. The battery is controlled via the Greenlight Innovations G12-200 multichannel battery test station described in the previous chapter.

The temperature profile within the HDPE slab depends on its thermal properties; inaccuracies in the thermal properties can lead to error in the measurements. Due to the variance in thermal conductivity provided by various suppliers of HDPE material, the thermal conductivity of the HDPE material is measured according to ASTM E1225-09 [5]. From ASTM E1225-09, the thermal conductivity of a material can be determined through the measurement of the materials' thermal resistivity. Detailed design of the experiment

used to measure the thermal resistivity can be found in Reference [79]. The thermal resistance R_t of the sample can be determined by measuring the temperature drop across a sample due to an applied heat flux on the surface of the sample, such that [5, 79],

$$R_{\mathrm{t}} = \frac{\Delta T}{Q} \tag{3.4}$$

where ΔT is the temperature difference over the thickness of the sample due to the imposed heat flow Q (W) in the fluxmeter.

Nine samples of varying thickness were cut from the same material used to make the calorimeter, with the thermal resistivity of each sample measured twice at separate times. The measured thermal resistance values comprise of contact resistance as well as the thermal resistivity of the material. The actual thermal resistance of the material can be found by applying a linear fit to the measured thermal resistivity values for samples of varying thickness, and extrapolating the value a sample of thickness of zero [79]. The measured thermal resistance values, with a corresponding linear fit are shown in Figure 3.3. The thickness measurements were performed by Fowler IP54 Electronic Disk Micrometer, accurate to $\pm$ 0.001 mm. With knowledge of the thermal resistivity of the material, the thermal conductivity can be calculated as,

$$k = \frac{L}{R_t A} \tag{3.5}$$

where k ($\mathrm{Wm^{-1}K^{-1}}$) is the thermal conductivity of the sample, L (m) is the thickness of the sample, and A ($\mathrm{m^2}$) is the surface area of the sample. The measured thermal conductivity of the sample is 0.53 $\mathrm{Wm^{-1}K^{-1}}$, which is within the range of published thermal conductivity value for the HDPE material.

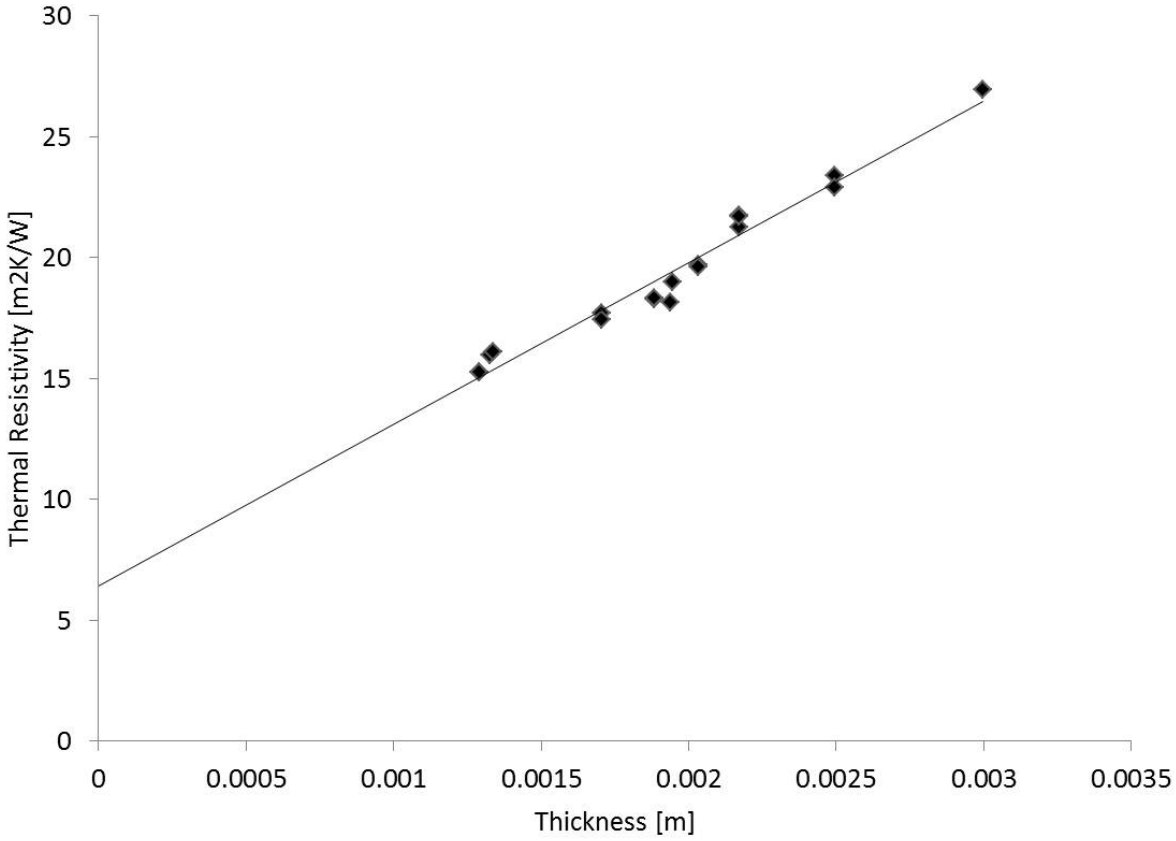

Figure 3.3: Thermal resistivity measurements of the High Density Polyethylene slab

Ten cubes measuring 25.4cm by 25.4cm by 25.4cm of HDPE were cut from the same material that was used to make the calorimeter in order to determine the HDPE material density. The dimensions were measured using the aforementioned Fowler micrometer, and the weight of the samples were measured by Denver Instruments TP-323 scale ($\pm$ 0.003g). The density of the samples were measured to be 956.91 kgm^{-3}. The specific heat of the HDPE material does not vary greatly within the range of tested temperatures, and is taken as 2.25 kgkJ^{-1}K-1 (specific heat of the material at 23°C) [64].

3.3 Experimental Condition and Procedure

The discharge rates will be described in terms of C-rates, where 1C is the discharge rate at which the battery will be fully depleted in one hour of operation (20A for the test battery), 2C the rate at which the battery is fully depleted in 30 minutes (40A), etc. The heat generation rates will be measured for five different battery discharge rates (0.25C, 0.5C, 1C, 2C, 3C), at six operating temperatures from -10°C to 40°C in 10°C increments. The battery is cycled five times to the cut-off voltage of 2.6V before testing, which allows irreversible capacity fade that may be present in unused Li-ion batteries to occur [34].

At the end of discharge, the battery is allowed to rest for two hours before being charged back to the open circuit voltage of 3.6V at a C/5 charge rate under a constant voltage constant current charging scheme. Following the completion of charge, the battery is allowed to rest for an hour to ensure the equilibration of battery chemistry. The details of the charge and discharge schedule can be seen in Figure 3.4.

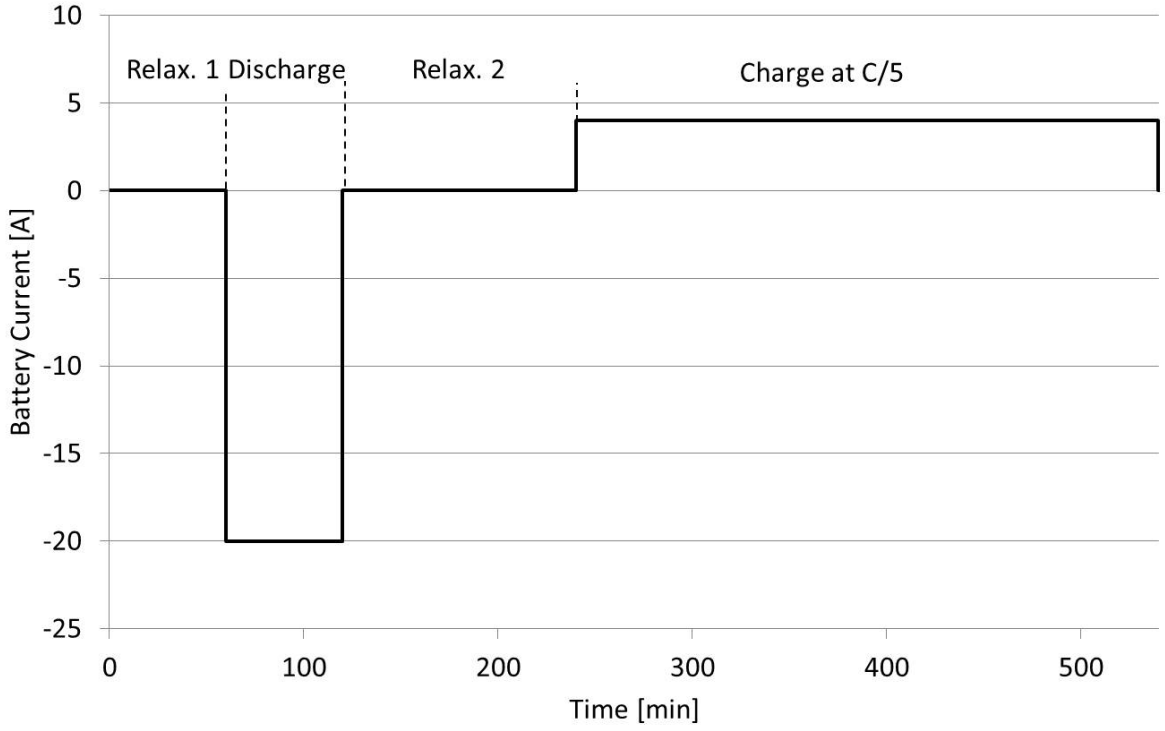

Figure 3.4: Test schedule used in the present study for charging and discharging of the Li-ion battery.

3.4 Data Reduction

In calorimetry applications, the heat generation rate of an object is unknown, but a temperature change within the calorimeter material of known thermal properties due to the generated heat can be measured. This measured temperature change allows the unknown heat generation rate to be inferred through the convolution theorem [33]. Applying the convolution theorem together with an assumption that the system response is linear, the overall measured change in temperature, $\Delta T_m(t)$, of the calorimeter due to the battery's unknown heat generation, $\dot{q}(t)$, is defined as the sum of the responses of the system to a series of discrete pulses from t_o to t, which form a temporal discretization of the heat

generation rate [33]. This can be written as the convolution integral [33],

$$\Delta T_m = \int_{t_o}^{t} \dot{q}(\tau)\phi(t-\tau)\mathrm{d}(\tau) \tag{3.6}$$

where $\phi(t-\tau)$ is the apparatus function, which can be defined as the response of the apparatus to a pulse heat generation. The apparatus function is typically measured through the system response to a pulse in a calibrated heater. With a known apparatus function, the real event of heat generation can be solved for by the deconvolution of Equation (3.6) either by using the Fourier transform or the recursion method [33]. Solving Equation (3.6) by Fourier transforms can lead to results that show periodicities and fluctuations that do not reflect the actual processes being measured, and the application of recursion method does not converge for all heat generation events, especially for abrupt changes and steps [33]. Since both solution methods use a measured apparatus function, errors in measurement while obtaining the apparatus function are propagated forward in calculations of actual heat generation rate.

In this thesis, obtaining the real event from the measured response of the system is done by treating the problem as an inverse heat conduction problem (IHCP). IHCP is similar to the aforementioned recursion method, but is distinct in two main ways: (*i*) the method does not require a measured apparatus function, which eliminates the propagation of error due to measurement of the apparatus function; (*ii*) the problem is broken down into two separate and equal heat conduction problems where the volumetric heat generation rate of the battery is determined as heat fluxes applied to the contact area between the HDPE slab and the battery.

The experimental apparatus utilizes two HDPE slabs as the heat conduction medium. The aluminium slabs are assumed to be at the temperature of the thermal bath due to its high thermal conductivity compared to the HDPE slabs. Due to the aforementioned form of the battery, the heat generated by the battery flowing through the calorimeter material can be assumed to be one dimensional, such that the total heat generated by the battery, $\dot{q}$, is equivalent to two separate and equal heat fluxes, q'', applied by the battery onto the calorimeter material. Heat diffusion equations describing the calorimeter can be set up as shown in Figure 3.5.

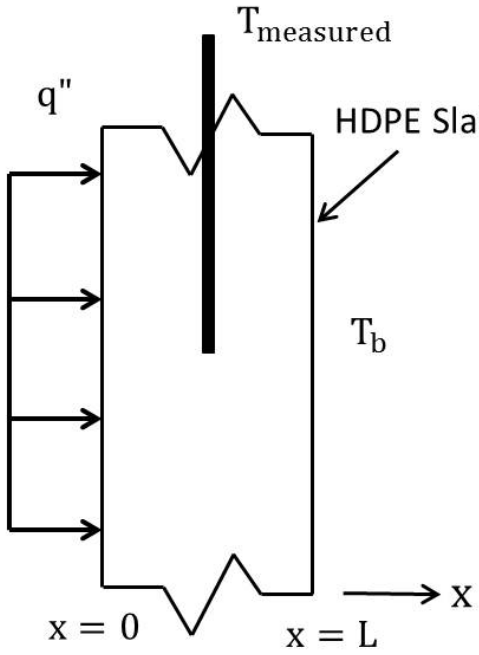

Figure 3.5: Problem setup for the measurement of inner temperature of the high density polyethylene (HDPE) slab T_{measured} from an imposed surface heat flux $\dot{q}''$ due to the heat generated in the test battery.

The measured temperature change at a specific location within the HDPE slabs due to the imposed heat flux ($\dot{q}''$) by the battery can be defined as T_{measured}. The temperature distribution within the HDPE slab is governed by Fick's law, and the following boundary and initial conditions

$$\begin{aligned} \frac{\partial^2 T}{\partial^2 x} &= \frac{1}{\alpha}\frac{\partial T}{\partial t} \\ T(x,0) &= T_{\text{b}} \\ T(L,t) &= T_{\text{b}} \\ -k\frac{\partial T}{\partial x}(0,t) &= q'' \end{aligned} \tag{3.7}$$

where α (m^2s^{-1}) is the thermal diffusivity of the calorimeter material (HDPE in the present study), subscripts 0 and L denote the locations on the HDPE slabs at the contact with the

battery and the aluminium slab respectively, and the subscript b denotes the temperature of the constant temperature bath. The temperature of the aluminium slabs can be assumed to be the same as the bath temperature due to its high thermal conductivity. The temperature increase at the measurement location x within the HDPE slab for a unit step increase in heat flux has to be found, such that

$$\Delta T_m = T_x(t) - T_b = q''[\phi(x,t)] \tag{3.8}$$

where $\phi(x,t)$ is the temperature rise at point x due to the applied heat flux. $\phi(x,t)$ can be found by solving the governing equations (Equation (3.7)) and (3.8), such that

$$\begin{aligned} T_x(t) - T_\mathrm{b} = q'' \Bigg[\sum_{n=1}^{\infty} \frac{-1}{k} \left[\frac{8(-1)^{1+n} L}{\pi^2(4n^2 - 4n + 1)} \right] \sin\left(\frac{(2n-1)\pi x}{2L} \right) \\ \exp\left(- \left[\frac{(2n-1)\pi}{2L} \right]^2 \alpha t \right) + \frac{x}{k} \Bigg] \end{aligned} \tag{3.9}$$

The convolution theorem can be applied using the apparatus function and the measured temperature change within the heat conduction medium. Owing to the discrete nature of the thermocouple measurements, $T_x(t)$, a discretized approximation of the convolution integral can be written as [11]

$$T_x(t) - T_b = \sum_{n=1}^{M} q''_n \big[\phi(x, t_{M-n+1}) - \phi(t_{M-n}) \big] \tag{3.10}$$

Inverse heat conduction problems (IHCP) use a measured temperature change within a material of known thermal properties to infer a heat flux that is applied to one of the boundaries [11]. IHCPs are ill-posed, owing to the divergence of its solutions which may occur due to small perturbations in the measured temperature from either noise or random errors in the experiment [10, 85]. For this study, Beck's Sequential Function Specification Method (Beck's Method) is used to introduce stability in the IHCP solution [11]. Beck's method increases the stability by introducing additional information about the problem by specifying that the solution is temporally smooth. The method assumes that the unknown heat flux $\dot{q}''$ is temporarily fixed over a number of future time steps, r, with each time step

having a period of Δt. Using Beck's Method, Equation (3.10) can be written in matrix form as [11]

$$\begin{pmatrix} \Delta\phi_0 & & & & & \\ \Delta\phi_1 & \Delta\phi_0 & & & & \\ \vdots & \vdots & \ddots & & & \\ \Delta\phi_{M-1} & \Delta\phi_{M-2} & \cdots & \Delta\phi_0 & & \\ \Delta\phi_M & \Delta\phi_{M-1} & \cdots & \Delta\phi_1 & \Delta\phi_0 & \\ \Delta\phi_{M+r-1} & \Delta\phi_{M+r-2} & \cdots & \cdots & \Delta\phi_1 & \Delta\phi_0 \end{pmatrix} \begin{pmatrix} q_1 \\ q_2 \\ \vdots \\ q_M \\ q_{M+1} \\ q_{M+r-1} \end{pmatrix} = \begin{pmatrix} T_1 \\ T_2 \\ \vdots \\ T_M \\ T_{M+1} \\ T_{M+r-1} \end{pmatrix} \tag{3.11}$$

The matrix of $\Delta\phi$'s represent the apparatus functions, which have been derived analytically from Equation (3.9). The matrix of T's represent the measured temperature change within the HDPE slabs due to the heat flux applied by the battery. The unknown heat flux at the surface of interest can be calculated using matrix manipulation techniques, after which it is then integrated to obtain the transient total heat generation rate of the battery. Exact solution to Equation (3.11) is obtained with a r value of 1, and the smoothness of the solution is increased with increasing values of r. An increase in r causes a decrease in sensitivity of the calculated heat flux at the surface of the HDPE slabs to oscillations in the temperature measurements, introducing more stability into the solution. Increased r values can also cause increased bias and decreased resolution in the calculated profile $\dot{q}''$, decreasing the values of the peaks in heat measurement. Therefore, the tuning parameters in Beck's Method needs to be carefully tuned to provide accurate results.

To tune the parameters in Becks method, Woodbury and Thackur defined a 'look ahead parameter', p, as [85]

$$p = r\Delta t \tag{3.12}$$

and showed that the calculated heat flux at the surface of interest has the same resolution and bias regardless of the value of r and Δt as long as p remains constant [85]. They concluded that adjustments need to be made to p such that the RMS error of the predicted temperature at any arbitrary location within the material is equivalent to the amount of noise in the measured data [85]. While manufacturer provided values for measurement errors can be used, Woodbury suggested experimentally determining the measurement

errors to increase accuracy in ascertaining the value of p, which is the approach adopted in the presented study and will be described in the following section [85].

3.5 Calibration

Noise in the temperature readings and steady state error of the calorimeter is determined using a controllable pseudo battery. The pseudo battery is made using a silicone heating pad (Omega Inc SRFR-609) with the same dimensions as the battery. The heat generation rate of the pseudo battery is controlled via a variable voltage supply (Keithley 2700). Calibration tests are performed with a heater output of 10W for two hours, during which the response of the system reaches steady state. After two hours, the heater is turned off, creating a step down in heat generation rate. The calorimeter is allowed to return to the initial conditions, and the calibration process is repeated for all the operating temperatures of the battery tests.

The standard deviation of the temperature measurements over 1000 seconds after the calorimeter reached steady state is calculated for ten separate tests, with the same heat generation rate and operating temperatures. The standard deviation values of the ten tests are averaged and calculated to be 0.025°C. Smoothing parameter p can be tuned using the obtained value of measurement error. Beck's method is applied to the temperature measurements with various values of p in order to calculate the heat flux at the surface of interest. The calculated heat flux is then used in Equation (3.9) to calculate the projected temperature at a distance of 4mm away from the surface of interest (same location as the thermocouple). Parameter p is adjusted such that the RMS error of the projected temperature matched the standard deviation of the actual temperature measurement, with the final, adjusted value of p being 100.

Beck's method (with $p = 100$) is applied to the measured temperature data to calculate the applied heat flux at the surface of interest for all operating temperatures tested. A comparison between the calculated heat generation rate using Beck's method and the actual heat generation rate of the heater at an operating temperature of 10°C is shown in Figure 3.6. The difference in the surface temperatures of the pseudo battery at the beginning of validation test and the step down event in heat generation signifies that there is stored

heat in the pseudo battery. The calculated heat generation rate using Beck's Method is capable of detecting the step down event in the heat output of the pseudo battery despite of the stored heat.

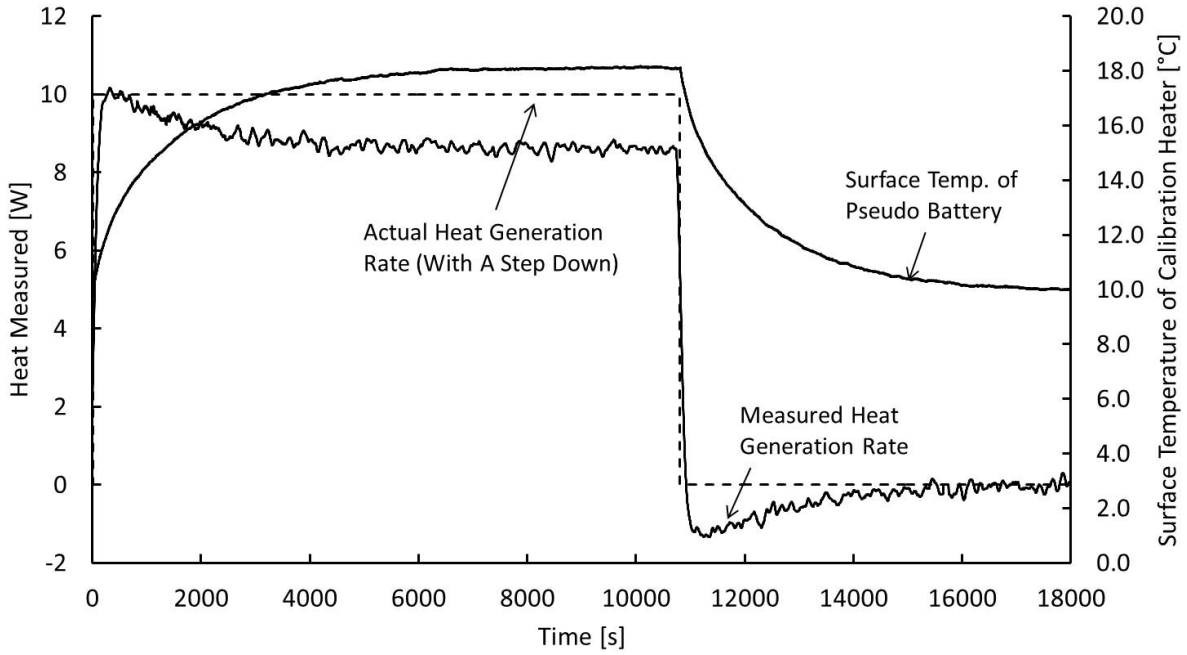

Figure 3.6: Comparison of the measured heat generation rate using Beck's Method (solid line) and the actual heat output from calibration heater (dashed line) at 10°C for a step down in heat output. Surface temperature refers to the temperature measured at the contact surface between the pseudo battery and the high density polyethylene (HDPE) slab.

The calibration process is repeated for all the operating conditions of the calorimeter with the same heat input, the results of which are shown in Table 3.1. It is seen that accuracy is between 80% and 85%, and on average, the heat lost to the environment which the calorimeter cannot account for is approximately 2W.

Table 3.1: Accuracy and standard deviation of heat generation measured by battery calorimeter for varying operating temperatures

Operating Temp.	40°C	30°C	20°C	10°C	0°C	-10°C
Accuracy	81%	84.4%	83.8%	84.1%	82.0%	80.1%
Standard Deviation	0.061W	0.052W	0.020W	0.041W	0.017W	0.066W

Chapter 4

Results and Discussion

The $LiFePO_4$ battery is tested as described in Section 2.2. All results shown in this section are average measurements of five repetitive tests. The maximum standard deviation in battery voltage throughout discharge for all tested operating temperatures is 0.13V for 3C discharge, while the open circuit voltage of the test battery is 3.6V.

From Equation (3.1) and (3.2), the rate of heat generation is dependent on two main parameters, discharge current and battery temperature. The following sections will summarize the observed effects of both battery discharge rate and operating temperature on battery heat generation rates.

4.1 Effect of Discharge Rate on Heat Generation Rate

Figure 4.1 shows the measured heat generation rates of the battery for all tested discharge rates at 20°C as a function of depth of discharge (varying from 0 to 1). There is a clear increase in battery heat generation throughout discharge at increased rates of discharge due to the higher irreversible heat generation. Irreversible heat generation is shown in Equation (3.1) and (3.2) as a function of current squared, whereas reversible heat generation is a linear function of current; therefore increasing the discharge current causes a corresponding

change in the proportion of the irreversible heat generation in the total heat generation of the battery. The total battery heat generation at 0.25C is shown to be almost negligible when compared to the total amount of heat generated when the battery is discharged at 3C at 20°C.

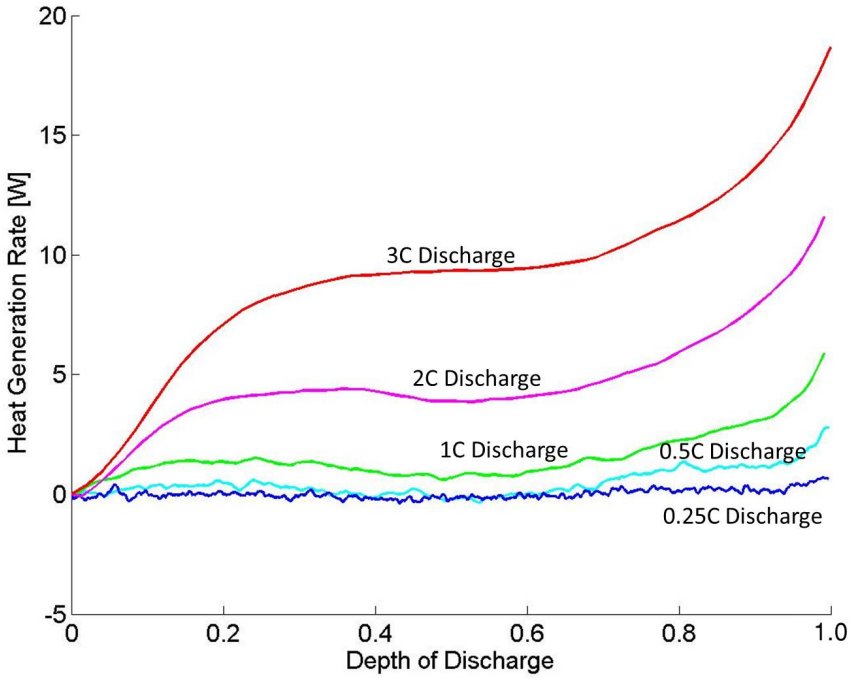

Figure 4.1: Effect of tested discharge rates on the heat generation rate of an A123 $LiFePO_4$ battery at an operating temperature of 20°C.

The heat generation can be non-dimensionalized by dividing the heat generated during battery discharge by the instantaneous amount of electrical power drawn from the battery. Non-dimensionalized heat generation provides a clearer representation of the heat generation characteristics throughout the discharge test, as shown in Figure 4.2. It can be seen that the proportion of heat generated to the instantaneous power drawn from the battery is under 0.10 for all discharge rates, regardless of discharge current. This shows that the proportion of electrical energy lost due to conversion to waste heat is on the same order of magnitude for all discharge rates.

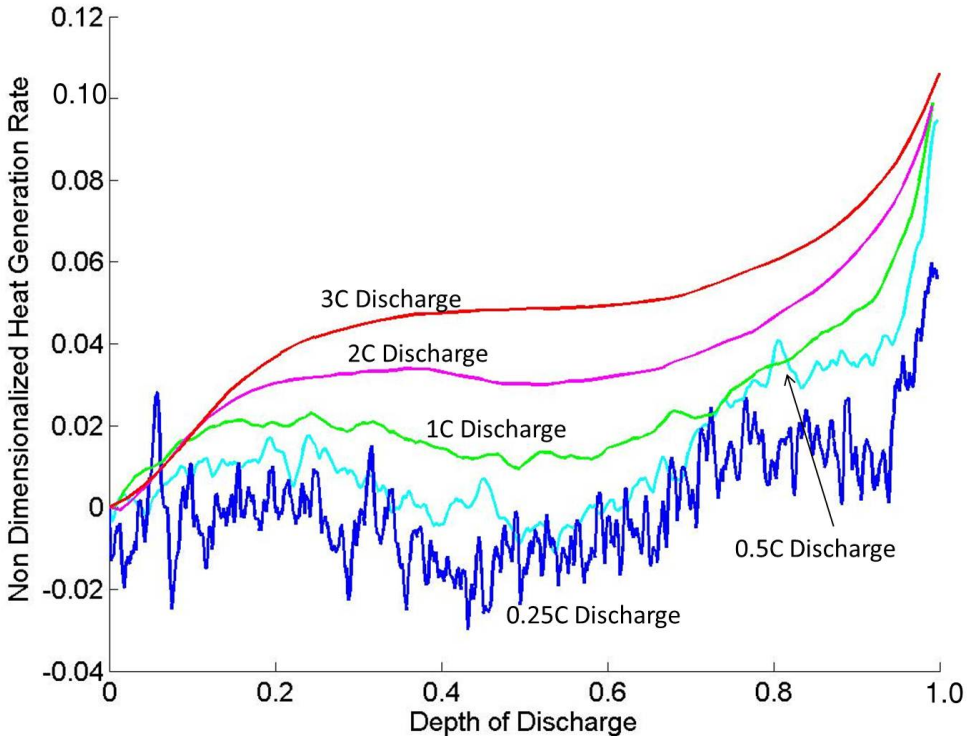

Figure 4.2: Effect of discharge rate on the heat generation rate, non-dimensionalized by electrical power drawn, of A123 $LiFePO_4$ battery at an operating temperature of 20°C.

The increase in non-dimensionalized heat generation at the higher rates of discharge can be related to two main factors: increased Joule heating at the battery current collectors and increased battery overpotentials at higher rates of discharge. Increases in battery discharge current directly increases the amplitude of the Joule heating due to increased current density near the current collectors. The overpotentials of the battery increase as the current drawn from the battery is increased according to the Tafel equation [67]. There is an increased amount of noise in the determined heat generation value for discharge rates less than 1C, caused by increased noise to signal ratio at lower battery heat generation rates.

As the discharge rate of the battery is decreased to less than 1C, irreversible heat generation (which is always exothermic) is reduced, and endothermic heat flow due to reversible heat generation can be observed in the measured heat generation curves. Figure

4.3 shows the heat generation profile at 0.5C discharge rate with the corresponding voltage discharge curves. Endothermic heat flow for 0.5C discharge rate can be observed for the battery operating temperatures of 30°C and 40°C. At a 0.25C discharge rate, endothermic heat flow during discharge can be observed for the battery operating temperatures from 0°C to 40°C (See Appendices for details).

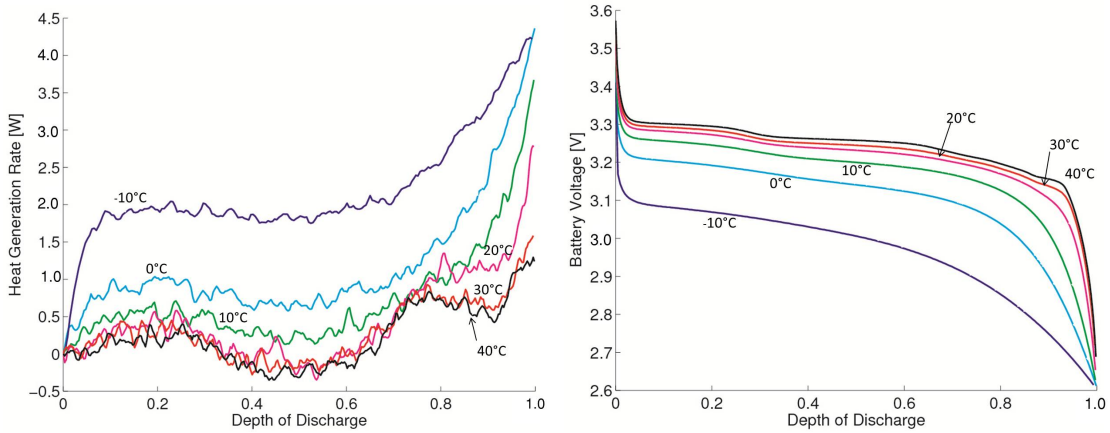

(a) Heat generation (b) Battery discharge curve

Figure 4.3: Effect of battery operating temperature on (a) heat generation rate and (b) battery discharge curve for an A123 $LiFePO_4$ battery at 0.5C discharge.

Non-uniform current distribution and concentration gradients on the electrodes due to limits in mass transfer can cause heat of mixing, which could be endothermic during the discharge [76]. The development of current and concentration gradients in the battery is caused by high discharge rates required of Li-ion batteries due to sudden EV acceleration. The amount of heat absorbed during the formation of the gradients will be released after the end of battery discharge, as the developed gradients relax to equilibrium. Heat of mixing increases at higher rates of discharge, and has been cited as a significant contributor to battery heat generation at discharge rates higher than 1C [2, 76].

As the battery discharge stops (and i goes to zero in Equation (3.1) and (3.2)), the heat generated by the battery should theoretically go to 0. Therefore, the existence of heat of mixing can be confirmed by examining the heat generation characteristics of the battery after the end of discharge. Figure 4.4 shows the existence of heat generation after

battery discharge terminates at 1C and 20°C where the heat generated by the battery after the end of discharge is representative of 16% of the total heat generation. It is shown in Section 3.5 that the data reduction technique is capable of detecting a step down in heat generation rate despite heat stored in the calibration test apparatus, therefore it is unlikely the observed heat generation phenomenon is due to the stored heat in the system.

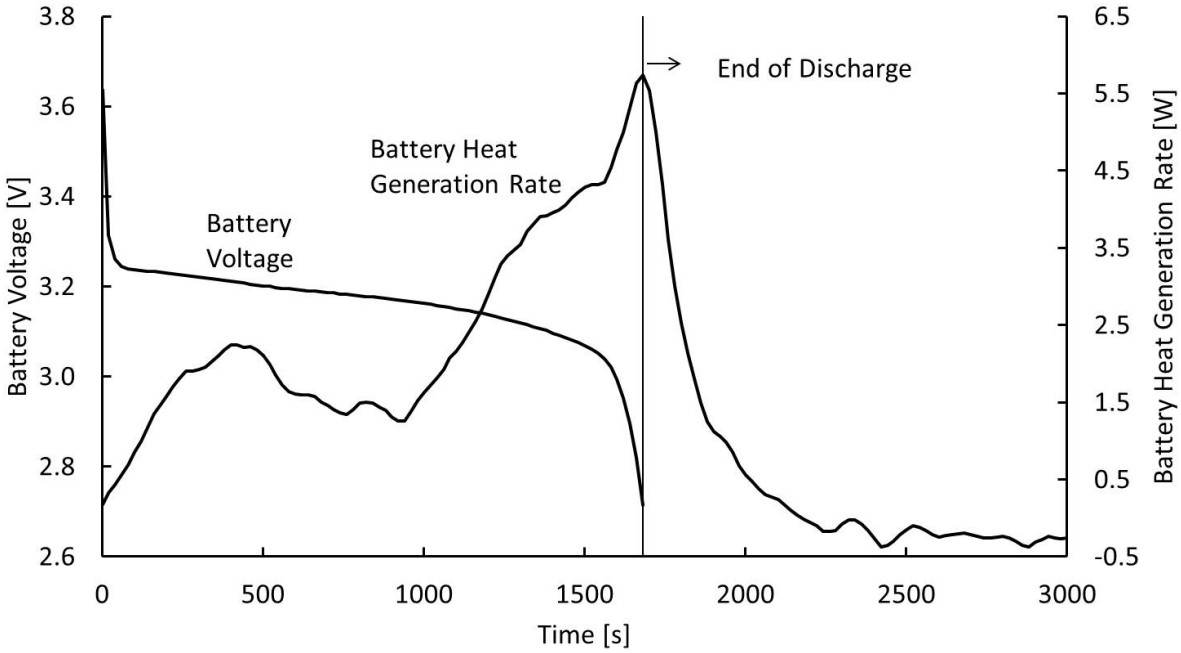

Figure 4.4: Battery discharge curve and measured heat generation profile of an A123 $LiFePO_4$ battery, for 1C discharge at 20°C. Measurements show the presence of additional heat generation post end of discharge.

Heat of mixing has been observed for small cylindrical Li-ion batteries, though only for discharge rates higher than or equal to 1C [2, 34]. The contribution of heat of mixing to the total heat generation of small cylindrical Li-ion batteries is generally neglected for discharge rates lower than 1C [8, 54]. For this study, the heat of mixing can be observed for the lowest discharge rate tested (0.25C), at both 40°C and -10°C, as seen in Figure 4.5a and Figure 4.5b respectively. Heat generation after the end of discharge contributes significantly to the total heat generated by the battery, accounting for 13% of the total

heat generation at -10°C. Therefore, heat of mixing for large prismatic Li-ion batteries should not be ignored at discharge rates higher than 0.25C.

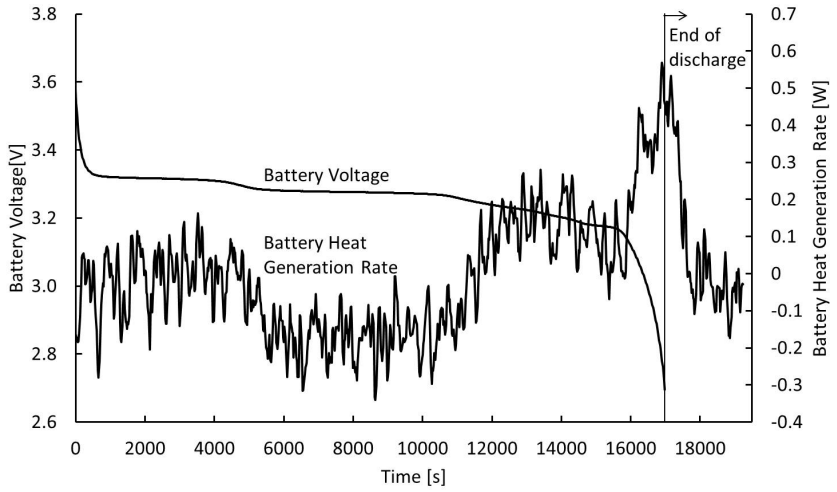

(a) 40°C

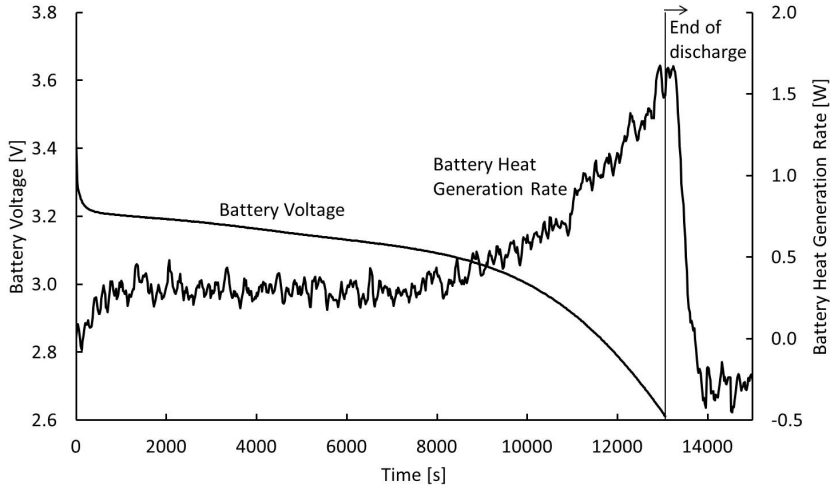

(b) -10°C

Figure 4.5: Battery discharge curve and measured heat generation profile of an A123 $LiFePO_4$ battery, at 0.25C discharge, showing battery heat generation post the end of discharge for operating temperatures of (a) 40°C, and (b) -10°C.

4.2 Effect of Operating Temperature on Heat Generation Rate

Figure 4.6a shows the battery heat generation rate profiles at various battery operating temperatures for a 1C discharge rate. It is seen that heat generation rates are greatly increased at lower temperatures, signifying the degradation of battery performance substantially. The heat generation rates of the battery at 30°C and 40°C is very similar at a 1C discharge rate, which shows increased proportion of the reversible heat generation in the total heat generation rate of the battery.

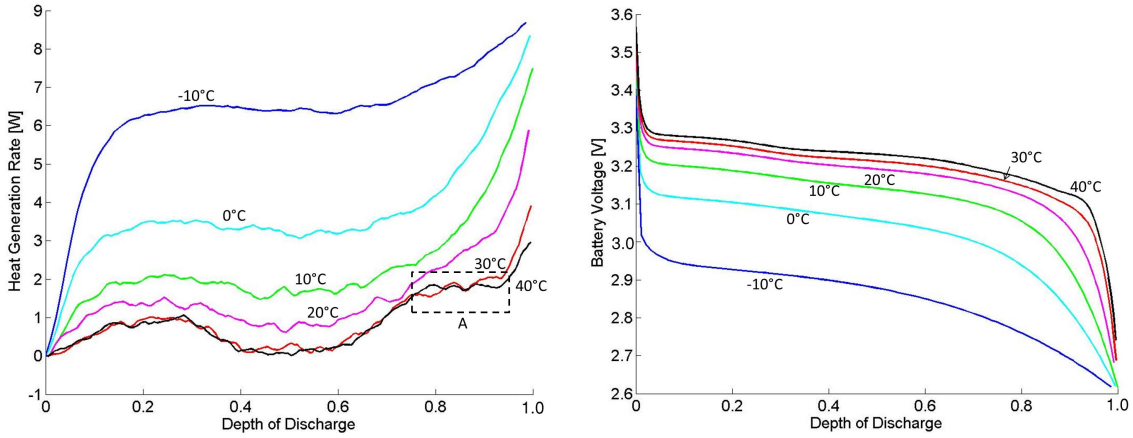

(a) Heat generation

(b) Battery discharge curve

Figure 4.6: Effect of battery operating temperature on (a) the heat generation rate and (b) the battery discharge curve of an A123 $LiFePO_4$ battery, for 1C discharge.

Battery internal resistance, the main cause of the irreversible heating in Equation (3.1), is dependent on the temperature. Previous work on small, cylindrical Li-ion batteries has shown a strong dependence of battery internal resistance on temperature, and the increase in battery internal resistance at low temperatures causes an increased amount of irreversible heat generation [40, 42, 44]. Decreased battery heat generation at higher operating temperatures is also due to increased rates of mass transport and reduced activation loss which decreases overpotential during discharge. Decreased overpotential translates to the diminished rates of irreversible heat generation at the beginning of discharge.

Battery discharge curves corresponding to the heat generation profiles at 1C discharge for all tested operating temperatures can be seen in Figure 4.6b. Discharge from -10°C to 20°C shows quasi-linear voltage drops with respect to depth of discharge, similar to what is commonly seen in literature. At battery operating temperatures higher than 20°C, two low frequency fluctuations in battery discharge curve are visible, the first of which occurs at a DOD of approximately 0.3, and the second at a DOD of approximately 0.8. This phenomenon has not been seen in literature for $LiFePO_4$ battery; it is commonly seen in Li-ion batteries of $LiMnO_4$ chemistry, and is caused by phase change mechanisms during discharge [8, 45].

As the amount of irreversible heat decreases at higher battery operating temperatures, additional features in the heat generation profile is more visible. Figure 4.6a shows a distinct decrease in heat generation at a depth of discharge (DOD) of approximately 0.3, with heat generation reaching a minimum at a DOD of approximately 0.5 for all battery operating temperatures. At battery temperatures of 0°C, 10°C, and 20°C, the decreased rate of heat generation causes the overall measured heat generation profile to form a distinct S-shape, with a single peak in exothermic heat flow during discharge. For operating temperatures higher than 20°C, a plateauing of heat generation is observed at a DOD of approximately 0.8 (shown as area A in Figure 4.6a). A comparison of the heat generation profiles of the battery at 0°C and 40°C is shown in Figure 4.7. The secondary plateau in heat generation rate can be observed for all discharge rates tested at 40°C, as shown in Figure 4.7a, but is not visible for battery operating temperature of 0°C (Figure 4.7b). This shows the dependence of the observed secondary plateauing phenomenon on the operating temperature of the battery.

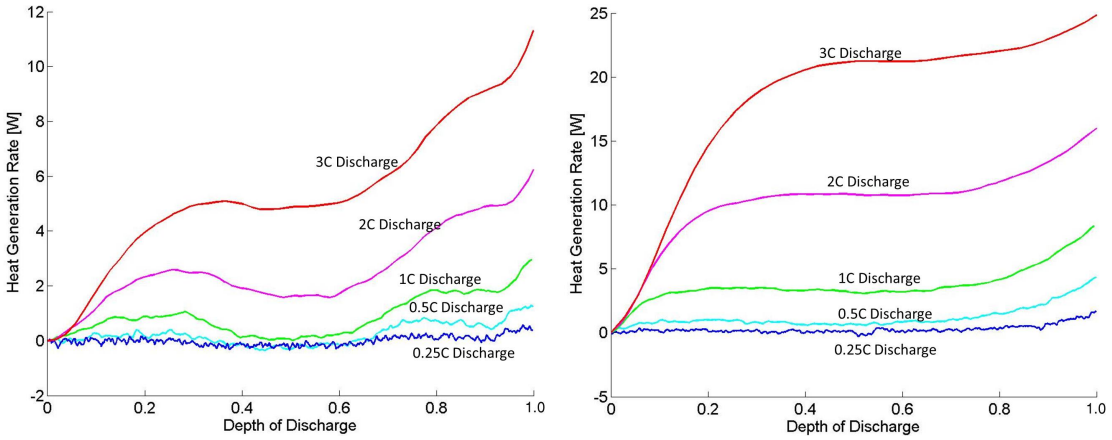

(a) 40°C (b) 0°C

Figure 4.7: Heat generation rate of an A123 $LiFePO_4$ battery at (a) 40°C and (b) 0°C for all tested discharge rates. Secondary plateauing in heat generation rate at a depth of discharge of 0.8 can be observed for all discharge rates tested at 40°C.

The observed features in the heat generation profile of the battery is more discernible at high battery operating temperatures. The transitions between plateaus in the battery discharge curve correspond to rapid change in the measured heat generation rates of the battery for 0.25C discharge at 30°C and 40°C, as seen in Figure 4.8.

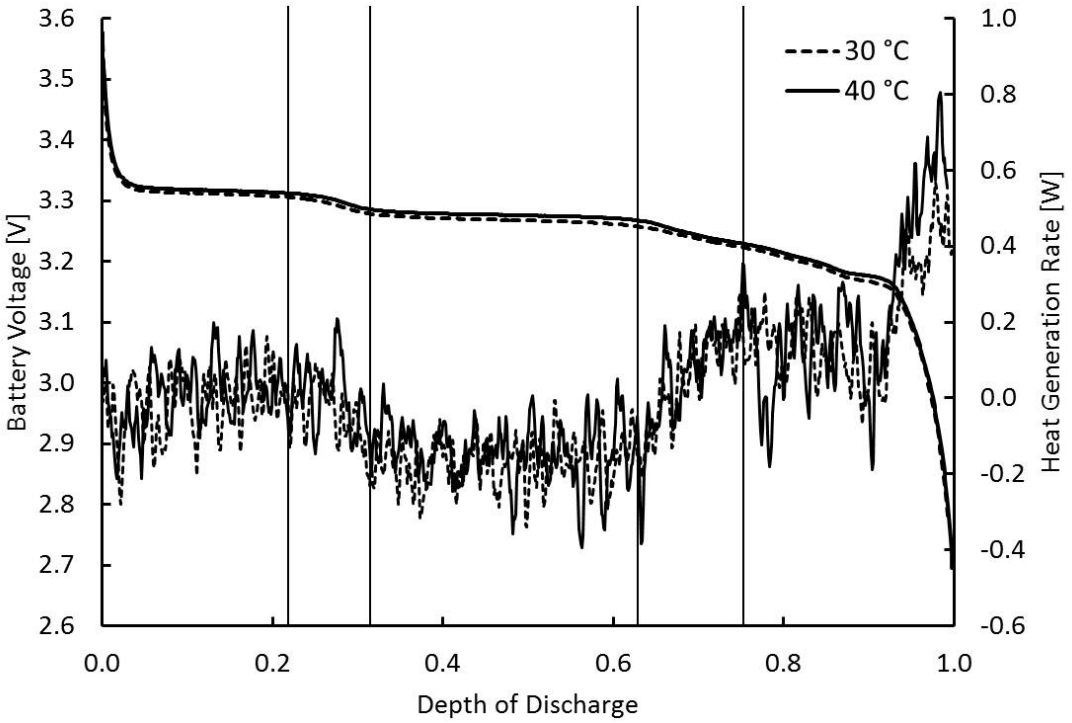

Figure 4.8: Heat generation rates and battery discharge curves for 0.25C discharge at 30°C and 40°C. Transitions between voltage discharge curve plateaus correspond to regions of rapid change in the measured battery heat generation.

The decrease in heat generation during discharge can be attributed to phase change mechanisms, which corresponds to transition regions between voltage plateaus in the battery discharge curves of $LiMnO_4$ batteries [3, 60]. Phase change mechanisms in $LiFePO_4$ remain a topic of investigation, with the existence of multiple models that are supported by experimental data [53]. Most models show the existence of only two phases in the phase change process [72, 87], although recent developments have shown the existence of transient phase changes through *in-situ* observations [61]. Double plateaus in voltage curve has been attributed to a double phase change in $LiMnO_4$ batteries [8, 45] which leads to the hypothesis that the presence of a double phase change is possible for $LiFePO_4$ batteries at higher battery operating temperatures at low discharge rates. The double plateau in the battery voltage for $LiFePO_4$ at higher battery operating temperatures have not been

reported in literature.

Through observations of heat generation phenomena in the tested $LiFePO_4$ battery, commonly used heat generation equations such as Equation (3.1) and (3.2) need to be modified to accurately model the complex heat generation characteristics of $LiFePO_4$ batteries. The fluctuations in heat generation rate and the double plateauing of the battery discharge curve at increased operating temperatures and decreased discharge rates warrants further investigation for better understanding of the phase change and heat generation mechanisms of large prismatic Li-ion batteries.

4.3 Validation of Results

The calculated heat generation rates of the battery using Beck's Method can be validated using the same experimental validation setup as discussed in Section 3.5. The pseudo battery comprising of the flexible silicone heater between two steel sheets takes the place of the actual battery inside the calorimeter, and its heat output is that of the measured heat generation rate of the actual battery. The temperature change within the HDPE slabs due to the heat generated by both the pseudo and test batteries are compared. A high coefficient of determination between the two system responses denotes that the measured heat generation rates of the test battery is accurate.

The measured heat generation rates of the test battery at 1C, 2C, and 3C discharge are used as heat output of the pseudo battery. Heat flow from the battery at discharge rates of 0.25C and 0.5C at high battery operating temperatures can be endothermic, which cannot be recreated by the pseudo battery and hence will be excluded from the validation tests. A comparison of the temperature increase between the validation and actual battery discharge tests at the temperature of 20°C is shown in Figure 4.9. At 20°C, the measured temperature increase within the HDPE slab for both the validation and battery discharge test is very close, achieving a R-squared value of above 0.99 for all discharge rates validated.

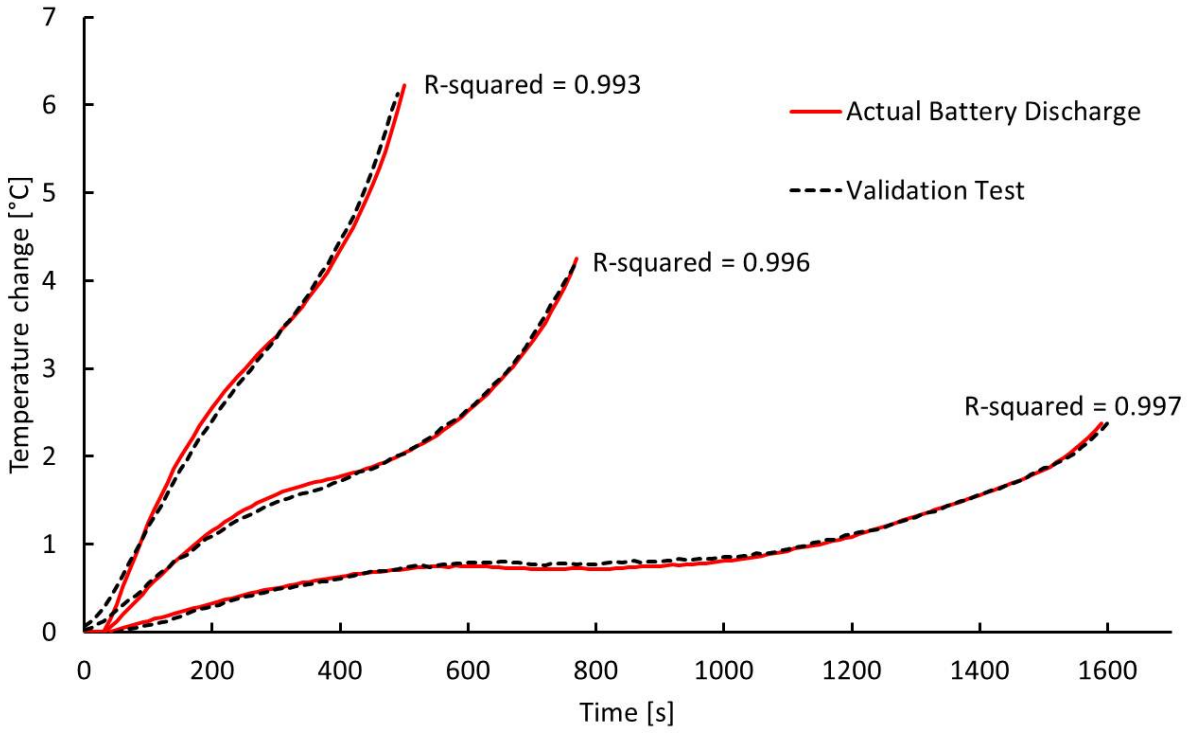

Figure 4.9: Comparison of the temperature measurements for the validation test and actual battery discharge for 1C, 2C and 3C discharge rates at an operating temperature of 20°C.

For other battery operating temperatures and discharge rates, the average temperature increase within the HDPE slab for the validation test and actual battery discharge achieve a minimum R-squared value of 0.98. The largest variations between the measured response of the calorimeter during real battery testing and pseudo battery testing occurs at high temperatures when the heat flow from the battery reaches near endothermic levels. This shows that the obtained results using Beck's method is a good representation of the actual heat generation rates of the battery for all operating temperatures and discharge rates investigated.

A summary of the measured total heat generation rates at the tested discharge rates and temperatures is shown in Table 4.1. The results are shown as a range due to the variation of heat generation rate of the battery throughout discharge. It can be seen that the minimum measured heat flow from the battery are endothermic at 0.25C discharge,

for the majority of tested temperatures. Complete heat generation curves throughout discharge for all tested discharge rates and battery operating temperatures are available in the Appendices.

Table 4.1: Summary of measured $LiFePO_4$ heat generation rates at all tested discharge rates and battery operating temperatures

Battery	Discharge Rate				
Temp.	0.25C	0.5C	1C	2C	3C
-10°C	0 - 2.09W	0 - 5.29W	0 - 10.82W	0 - 24.71W	—
0°C	-0.33 - 2.05W	0 - 5.20W	0 - 10.21W	0 - 19.52W	0 - 29.93W
10°C	-0.24 - 1.43W	0 - 4.37W	0 - 8.87W	0 - 16.72W	0 - 24.79W
20°C	-0.44 - 0.87W	0 - 3.32W	0 - 4.92W	0 - 13.78W	0 - 4.92W
30°C	-0.46 - 0.85W	-0.33 - 1.86W	0 - 4.56W	0 - 10.39W	0 - 16.48W
40°C	-0.43 - 0.71W	-0.44 - 1.62W	0 - 3.70W	0 - 7.88W	0 - 14.21W

Chapter 5

Conclusions

5.1 Summary

The work in this thesis can be broken into two sections. Firstly, a method of temperature control for large prismatic batteries using water-ethylene glycol mixture is developed for the accurate measurement of the battery discharge characteristics. It is shown for the tested battery, a prismatic A123 $LiFePO_4$ battery, that the temperature variation is limited to 0.3°C over the time of the battery characterization test (from the beginning to the end of the test) and 0.4°C over the battery surface (spatial change) at the high discharge rate of 3C. This is in contrast with the temperature variation of 13.1°C temporally and 4.3°C spatially when using the conventional method of battery temperature control through air convection under the same test condition. Battery capacity is significantly influenced by its operating temperature, and can have a difference of as much as 25% when using the two different methods of battery temperature control due to the significant temporal and spatial temperature differences during testing. The new method of temperature control developed can yield more accurate characterization of battery discharge due to the elimination of state-of-charge drift caused by spatial variations in battery temperature, and inaccurate discharge characteristics due to battery heat up at various discharge and operating conditions.

Battery characterization tests were performed at various operating temperatures using

the developed temperature control method. Low temperature operation of the battery shows a dramatic decrease in battery capacity, with a decrease of approximately 95% in available battery energy between battery discharged at 20°C and -10°C at a 3C discharge rate. Reduction in available battery energy is less dramatic at lower discharge rates, showing a decrease of approximately 36% at a discharge rate of 0.2C for the same temperature change in battery operating temperature. The results of battery testing show the importance of controlling the battery temperature at optimum levels, and the importance of characterizing the heat generation rates of the battery such that an effective thermal management system capable of holding the battery at these optimum temperatures can be designed.

A method of heat generation measurement for a prismatic battery is developed in the second part of the thesis, which is applicable to any prismatic battery regardless of chemistries. The heat generation rate of a 20Ah prismatic A123 $LiFePO_4$ battery is measured under a wide range of discharge rates and operating temperatures. It is shown that the heat generation rate of the tested battery increases with the discharge rate, and decreases with the operating temperature. Heat of mixing, which is ignored in literature for discharge rates lower than 1C is observed at a discharge rate as low as 0.25C for all tested battery operating temperatures. The magnitude of the heat of mixing at -10°C for 0.25C discharge accounts for 13% of the overall heat generated during discharge and hence cannot be ignored for prismatic $LiFePO_4$ batteries. Measured heat generation rates follow an S-shape profile, with exothermic heat flow at the beginning and end of discharge, and a decrease in heat generation rate at a depth of discharge of approximately 0.3. For rates of discharge lower than 1C, the decrease in heat flow is reduced to endothermic levels, especially at high battery operating temperatures. A visible secondary plateau in heat generation can be observed for increased battery operating temperatures at a depth of discharge of approximately 0.8. Transitions between the voltage discharge curve plateaus correspond to regions of rapid change in measured battery heat generation. Double plateaus in battery discharge curve show the possibility of a double phase change mechanism at lower rates of discharge for high battery operating temperatures.

The measured heat generation is validated by using a controllable power supply and a resistance heater, and it is shown that the present technique can accurately recreate the

heat generation of the battery under various discharge and operating conditions. The maximum heat generation measured from the battery is 30W, corresponding to a 3C discharge at 0°C.

5.2 Recommendations

This thesis has taken a step in characterizing the heat generation rate of the prismatic Li-ion at constant current discharge for different operating temperatures, as well as quantifying the effects of operating temperature on battery performance. Through the results presented, it was found that the widely used equations in simulations of battery heat generation are inadequate to accurately model the complex heat generation characteristics of the large prismatic Li-ion batteries. The presented method should be modified in order to decrease uncertainty in the measured results, and further work needs to be performed to better understand the heat generation characteristics of the battery at fluctuating levels of discharge, as seen in EV drive cycles.

Changes to the current calorimeter design that could potentially decrease uncertainty in results include:

1. Using more accurate temperature measurement devices to decrease bias and random errors. Manufacturer supplied thermocouple error is ± 0.1°C. Thermistors with accuracies of ± 0.01°C accuracy can be used in lieu of the thermocouples, which can significantly decrease the bias and random errors in temperature measurements. The bias and resolution of solution can be improved through additional tuning of the smoothing parameter in the solution method, since the decreased amount of perturbations and noise in the temperature measurements decreases the amount of smoothing required.

2. Increasing the number of embedded temperature measurement devices at the same location within the calorimeter. This would allow the response of the calorimeter to the same heat generation event to be measured by multiple measurement devices. The different measurements for the same event can be averaged, and the effect of random

errors from the measurement devices on the calculated heat generation curve would be reduced.

3. Low frequency filtering can be performed on the raw data to decrease the effect of low frequency noise on the calculated heat generation rate. Low frequency noise exists in the measured data due to the style of temperature control in the thermal bath. The amount of low frequency noise in the temperature data can be obtained from the signal by applying a high ordered polynomial curve fit to the temperature measurements [37]. This curve fit represents the low frequency oscillations in the data, which can then be subtracted from the actual temperature signal.

Changes to the current calorimeter design and testing procedures to increase functionality include:

1. Embedding additional temperature measurement devices at different locations in the calorimeter material, which can provide heat generation rates at various locations in the battery. This can be used to generate a surface plot of the heat generation rates of the battery, and can allow areas of high heat generation (especially around the current collectors) to be characterized.

2. Battery discharge schedule with non-constant rates of power draw such as those based on driving cycles can be used to measure rate of heat generation during real life driving conditions.

References

[1] S. Al Hallaj, H. Maleki, J.S. Hong, and J.R. Selman. Thermal modeling and design considerations of lithium ion batteries. *Journal of Power Sources*, 83:1–8, 1999.

[2] S. Al Hallaj, J. Prakash, and J.R. Selman. Characterization of commercial li-ion batteries using electrochemical-calorimetric measurements. *Journal of Power Sources*, 87:186–194, 2000. 32, 51, 52

[3] S. Al Hallaj, R. Venjatachalapath, J. Prakash, and Selman J.R. Entropy changes due to structural transformation in the graphite anode and phase change of the $licoo_2$ cathode. *Journal of the Electrochemical Society*, 147:2432–2436, 2000. 15, 16, 57

[4] D. Andre, M. Meiler, K. Steiner, C. Wimmer, T. Soczka-Guth, and D.U. Sauer. Characterization of high-power lithium ion batteries by electrochemical impedance spectroscopy. i. experimental investigation. *Journal of Power Sources*, 196:5334–5341, 2011. 14

[5] ASTM International. Standard Test Method for Thermal Conductivity of Solids by Means of the Guarded-Comparative-Longitudinal Heat Flow Technique, 2009. 36, 37

[6] A. Awarke, M. Jaeger, O. Oezdemir, and S. Pischinger. Thermal analysis of a li-ion battery module under realistic ev operating conditions. *International Journal fo Energy Research*, pages 1099–114x, 2012. 15, 16

[7] T. M. Bandhauer, S. Garimella, and T. F. Fuller. A critical review of thermal issues in lithium-ion batteries. *Journal of the Electrochemical Society*, 158:R1–R25, 2011. 2, 31, 32, 33

[8] H. Bang, H. Yang, Y. K. Sun, and J. Prakash. In situ studies of $li_xmn_2o_4$ and $li_xal_{0.17}mn_{1.83}o_{3.97}o_{3.97}s_{0.03}$ cathode by imc. *Journal of The Electrochemical Society*, 15:A421–A428, 2005. 33, 52, 55, 57

[9] F.F.C Bazito and R.M. Toressi. Cathodes for lithium ion batteries: The benefits of using nanostructured materials. *Journal of the Brazilian Chemistry Society*, 17:627–642, 2006. 4

[10] J.V. Beck, B. Blackwell, and A. Haji-Sheikh. Comparison of some inverse heat conduction methods using experimental data. *Internation Journal of Heat and Mass Transfer*, 39:3649–3657, 1996. 43

[11] J.V. Beck, B. Blackwell, and C.R. St-Clair. *Inverse Heat Conduction, Ill Posed Problems*. John Wiley and Sons, Inc, 1985. 43, 44

[12] D. Bernardi, E. Pawlikowski, and J. Newman. A general energy balance for battery systems. *Journal of the Electrochemical Society*, 132:5–12, 1985. 30

[13] G. Botte, B. Johnson, and R. White. Influence of some design variables on the thermal behavior of a lithium-ion cell. *Journal of the Electrochemical Society*, 146(3):914–923, 1999.

[14] P.G. Bruce, B. Scrosati, and J. Tarascon. Nanomaterials for rechargeable lithium batteries. *Angewandte Chemie*, 47:2930–2946, 2008. 4

[15] H.S. Carslaw and J.C. Jaeger. *Conduction of Heat in Solids*. Oxford University Press, 1959.

[16] S. Chacko and Y. Chung. Thermal modelling of li-ion polymer battery for electric vehicle drive cycles. *Journal of Power Sources*, 213:296–303, 2012. 15, 16

[17] L. Chen, K. Chen, and F. Sun. Research on thermo-physical properties identification and thermal analysis of ev li-ion battery. In *IEEE Vehicle Power Propulsion Conference*, pages 1643–1648, 2009. 2

[18] Y. Chen and J. Evans. Heat transfer phenomena in lithium/polymer-electrolyte batteries for electric vehicle application. *Journal of the Electrochemical Society*, 140:1833–1838, 1993.

[19] S.S. Choi and H. Lim. Factors that affect cycle-life and possible degradation mechanisms of a li-ion cell based on $licoo_2$. *Journal of Power Sources*, 111:130–136, 2002. 14, 27

[20] Tesla Motor Company. Purchasing facts, 2013. 1

[21] U.S. Advanced Battery Consortium. Electric vehicle battery test procedures manual rev. 2. Technical report, U.S. Advanced Battery Consortium, 1996.

[22] T.R. Crompton. *Battery Reference Book*. Elsevier Newnes, 2000. 5

[23] United States of America Department of Energy. One million electric vehicles by 2015, february 2011 status report. Technical report. 1

[24] S. Dhameja. *Electric Vehicle Battery Systems*. Newnes, 2004.

[25] A. Dinger, Martin R., X. Mosquest, Rabl. M., D. Rizoulis, M. Russo, and G. Sticher. Batteries for electric cars, challenges, opportunities, and the outlook to 2020. Technical report. 1

[26] Y. Duan and G.F. Naterer. Heat transfer in phase change materials for thermal management of electric vehicle battery modules. *International Journal of Heat and Mass Transfer*, 53:5176–5182, 2010.

[27] J.W. Fergus. Recent developments in cathode materials for lithium ion batteries. *Journal of Power Sources*, 195:939–954, 2010.

[28] M. Fleckenstein, O. Bohlen, M. Roscher, and B. Baker. Current density and state of charge inhomogeneities in li-ion battery cells with lifepo4 as cathode material due to temperature gradients. *Journal of Power Sources*, 196:4769–4778, 2011. 14, 15

[29] S. Gerssen-Gondelach and A.P.C Faaij. Performance of batteries for electric vehicles on short and longer term. *Journal of Power Sources*, 212:111–129, 2012. 3

[30] N. Gordon-Bloomfield. Independent tests show nissan leaf electric cars lost range in hot climates. Green Car Reports, September 2012. 2

[31] W.B. Gu and C.Y. Wang. Thermal-electrohemical modeling of battery systems. *Journal of the Electrochemical Society*, 147:2910–2922, 2000. 31

[32] C.H. Hamann, A. Hamnett, and W. Vielstich. *Electrochemistry, second, completely revised and updated edition*. Wiley, 2007. 5

[33] W. Hemminger and G. Hoehne. *Calorimetry, Fundamentals and Practice*. Verlag Chemie, 1984. 40, 41

[34] J.S. Hong, H. Maleki, S. Al Hallaj, L. Redey, and J.R. Selman. Electrochemical-calorimetric studies of lithium-ion cells. *Journal of the Electrochemical Society*, 145:1489–1591, 1998. 15, 16, 20, 32, 39, 52

[35] H. Horie, T. Abe, and T. Kinoshite. A study on advanced lithium ion battery system for evs. *World Electric Vehile Journal*, 2:25–30, 2008.

[36] A123 Systems Inc. Nanophosphate basics: An overview of the structure, properties and benefits of a123 systems proprietry lithium ion battery technology. Technical report. 5

[37] National Instruments Inc. Overview of curve fitting models and methods in labview. Technical report. 64

[38] F. Incropera and D.P. DeWitt. *Fundamentals of Heat and Mass Tranfer*. Wiley, sixth edition, 01.

[39] A. Ingram. Nissan leaf, how much does it lose in the cold. Green Car Reports, February 2013. 2

[40] Y. Inui, Y. Kobayashi, Y. Watanabe, and Y. Watase. Simulation of temperature distribution in cylindrical and prismatic lithium ion secondary batteries. *Eneregy Conversion Management*, 48:2103–2109, 2007. 54

[41] D.H. Jeon and S.M. Baek. Thermal modeling of cylindrical lithium ion battery during discharge cycle. *Energy Conversion and Management*, 52:2973–2981, 2011. 15

[42] H. Kameyama, T. Hanamoto, K. Ito, Y. Inui, and K. Onda. Study on heat generation behavior of small lithium ion secondary battery. *IEEE Transactions on Energy Conversion*, 112:1192–1199, 2002. 15, 16, 54

[43] G. Kim, A. Pesaran, and R Spotnitz. A three-dimensional thermal abuse model for lithium-ion cells. *Journal of Power Sources*, 170(2):476–489, 2007. 32

[44] J.H. Kim, S.J. Lee, J.M. Lee, and B.H. Cho. A new direct current internal resistance and state of charge relationship for the li-ion battery pulse power estimation. In *International Conference on Power Electronics*, pages 1173–1178, 2007. 15, 54

[45] J.S. Kim, J. Prakash, and J.R. Selman. Thermal characteristics of $li_xmn_2o_4$ spinel. *Electrochemical and Solid-State Letters*, 4:A141–A144, 2001. 32, 55, 57

[46] U.S. Kim, C.B. Shin, and C.S. Kim. Effect of electrode configuration on the thermal behavior of a lithium polymer battery. *Journal of Power Sources*, 180:909–916, 2008. 15, 31

[47] U.S. Kim, C.B. Shin, and C.S. Kim. Modeling for the scale-up of a lithium-ion polymer battery. *Journal of Power Sources*, 189:841–846, 2009. 31

[48] U.S. Kim, J. Yi, C.B. Shin, T. Han, and S. Park. Modelling the thermal behaviour of a lithium ion battery during charge. *Journal of Power Sources*, 196:5115–5121, 2011.

[49] Y. Kim and H. Ha. Design of interface circuits with electrical battery models. *IEEE Transactions on Industrial Electronics*, 44:81–86, 1997.

[50] Y. Kobayashi, H. Miyashiro, K. Kumao, T. Takei, K. Iwahori, and I. Uchida. Precise electrochemical calotimetry of licoo2/graphite lithium-ion cell. *Journal of the Electrochemcial Society*, 149(8):A978–A982, 2002. 33

[51] B.Y. Liaw, P. Roth, R. Jungst, G. Nagasubramanian, H. Case, and D. Doughty. Correlation of arrhenius behaviors in power and capacity fades with cell impedance

and heat generation in cylindrical lithium ion cells. *Journal of Power Sources*, 119:874–886, 2003.

[52] H.K. Liu, G.X. Wang, Z. Guo, J. Wang, and K. Konstantinov. Nanomaterials for lithium-ion rechargeable batteries. *Journal of Nanosciece and Nanotechnology*, 6:1–15, 2006. 4

[53] C. T. Love, A. Korovina, C.J. Patridge, K.E. Swider-Lyones, M.E. Twigg, and D.E. Ramaker. Review of lifepo4 phase transition mechanisms and new observations from x-ray absorption spectroscopy. *Journal of the Electrochemical Society*, 160:A3151–A3161, 2013. 57

[54] W. Lu, H. Yang, and J. Prakash. Determination of reversible and irreversible heats of li0.8co0.2o2/mesocarbon microbead li-ion cell reactions using isothermal microcalorimetry. *Electrochemica Acta*, 51:1322–1329, 205. 52

[55] E. Merkle. Ford cars, utilities and trucks all post u.s. sales gains in 2012. Ford Inverstor Relations News, January 2013. 1

[56] P.L. Moss, G. Au, E.J. Plichta, and J.P. Zheng. An electrical circuit for modeling the dynamic response of li-ion polymer batteries. *Journal of the Electrochemical Society*, 155:A986–A994, 2008.

[57] P. Nelson, K. Amine, and A. Rousseau. Advanced lithium-ion batteries for plug in hybrid electric vehicles. Technical report, Argonne National Laboratory, Argonne IL, 2000. 9

[58] Department of Energy and U.S. Environmental Protection Agency. Federal tax credits for electric vehicles purchased, 2013.

[59] Ontario Ministry of Transportation. Electric and hybrid electric vehicle program incentives, 2013.

[60] K. Onda, H. Kameyama, Hanamoto T., and K. Ito. Experimental study on the heat generation behavior of small lithium-ion secondary batteries. *Journal of the Electrochemical Society*, 150, 2003. 15, 16, 33, 57

[61] Y. Orikasa, T. Maeda, Y. Koyama, H. Murayama, K. Fukuda, H. Tanida, E. Arai, H. amd Matsubara, Y. Uchinoto, and Z. Ogumi. Transient phase change in two phase reaction between lifepo4 and fepo4 under battery operation. *Chemistry of Materials*, 25:1032–1039, 2013. 57

[62] M.N. Ozisik and H.R.B Orlande. *Inverse Heat Transfer*. Taylor & Francis, 2000.

[63] C.R. Pals and J. Newman. Thermal modeling of lithium/polymer battery. i. discharge behavior of a single cell. *Journal of the Electrochemical Society*, 142:3274–3281, 1995. 9, 14

[64] A.J. Peacock. *Handbook of Polyethylene, structures, properties, and applications*. Marcel Dekker Inc., 2000. 38

[65] G. Pistoria. *Lithium Batteries, new materials, developments, and perspectives*. Elsevier, 1994. 4

[66] P. Ramadass, B. Haran, P. Gomadam, R. White, and B. Popove. Development of first principles capacity fade model for li-ion cells. *Journal of the Electorchemistry Society*, 155:196–203, 2004.

[67] T.B. Reddy. *Linden's Handbook of Batteries*. McGraw-Hill Inc., 2011. ix, x, 3, 4, 5, 6, 7, 8, 50

[68] Y.F. Reynier, R. Yazami, and Fultz. B. Thermodynamics of lithium intercalation into graphites and disordered carbons. *Journal of the Electrochemical Society*, 151:A422–A426, 2004. 14

[69] S. Santhanagopalan, Q. Zhang, K. Kumaresan, and R. White. Parameter estimation adn life modeling of lithium ion cells. *Journal of the Electrochemical Society*, 155:A345–A353, 2008. 9

[70] C.M. Shepherd. Theoretical design of primary and secondary cells-part iii battery discharge equation. Technical report, Electrochemisty Branch, U.S. Naval Research Laboratory, 1963. 13

[71] SONY Co. *SONY Battery Manual for SONYUS18650*.

[72] V. Srinivasan and J. Newman. Discharge model for the lithium iron-phosphate electrode. *Journal of the Electrochemical Society*, 151:A1517–A1529, 2004. 57

[73] H. Sun, X. Wang, B Tossan, and R. Dixon. Three-dimensional thermal modeling of a lithium-ion battery pack. *Journal of Power Sources*, 206:349–356, 2012.

[74] J.M. Tarascon and M Armand. Issues and challenges facing rechargeable lithium batteries. *Nature*, 414:359–367, 2001. x, 9, 10

[75] MIT Electric Vehicle Team. A guide to understanding battery specifications. Technical report, MIT, 2008.

[76] K.E. Thomas and J. Newman. Heats of mixing and of entropy in porous insertion electrodes. *Journal of Power Sources*, 119:844–849, 2003. 7, 14, 51

[77] O. Tremblay and L. Dessaint. Experimental validation of a battery dynamic model for ev applications. *World Electric Vehicle Journal*, 3:1–10, 2009. 13, 14

[78] T. Trigg and P Telleen. Global ev outlook. Technical report. 1

[79] G. Unsworth, N. Zamel, and X. Li. Through-plane thermal conductivity of the microporous layer in a polymer electrolyte membrane fuel cell. *Internaltional Journal of Hydrogen Energy*, 37:5161–5169, 2012. 37

[80] K. Vetter, P. Novak, M.R. Wagner, C. Veit, K Moller, Besenhard J.O., M. Winter, M. Wohlfahrt-Mehrens, C. Vogler, and A. Hammouche. Ageing mechanisms in lithium-ion batteries. *Journal of Power Sources*, 147:269=281, 2005. 9

[81] A. Vlahinnos and S. Burch. Thermal performance of ev and hev battery modules and packs. Technical report, National Renewable Energy Laboratory, 2003.

[82] C.Y. Wang and V. Srinivasan. Computational battery dynamics (cbd)-electrochemical/thermal coupled modeling and multi-scale modeling. *Journal of Power Sources*, 110:364–376, 2002. 31

[83] J. White. To spark buyers for electric cars, drop the price to nearly $0. Wall Street Journal, May 2013.

[84] M.S. Whittingham. Lithium batteries and cathode materials. *Chemistry Review*, 104:4271–4301, 2004. 4

[85] K.A. Woodbury and S.K. Thackur. Redundant data and future times in the inverse heat conduction problem. *Inverse problems in Engineering*, 2:319–333, 1996. 43, 44, 45

[86] W. Wu, X. Xiao, and X Huang. The effect of battery design parameters on heat generation and utlization in a li-ion cell. *Electrochimica Acta*, 83:227–240, 2012. 31

[87] A. Yamada, H. Koizumi, N. Sonoyama, and Janno R. Phase change in lixfepo4. *Electrochemical and Solid State Letters*, 8:A409–A413, 2005. 57

[88] J. Zhang, S. Ci, and Alahmad. Shraif H. Modelling discharge behaviour of multicell battery. *IEEE Transactions on Energy Conversion*, 25:1133–1141, 2010.

[89] S.S. Zhang, K. Xu, and T.R. Jow. The low temperature performance of li-ion batteries. *Journal of Power Sources*, 115:137–140, 2003. 9, 14, 26

[90] X. Zhang. Thermal analysis of a cylindrical lithium-ion battery. *Electrochimica Acta*, 56:1246–1255, 2011.

Appendix A: Effect of Operating Temperature on Battery Discharge Curves

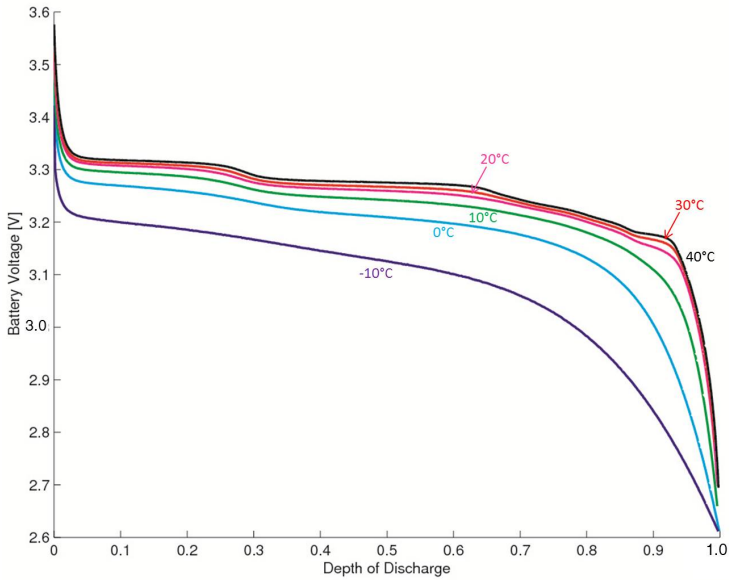

Figure 1: Effect of operating temperature on the discharge curve of the test battery at 0.25C constant current discharge

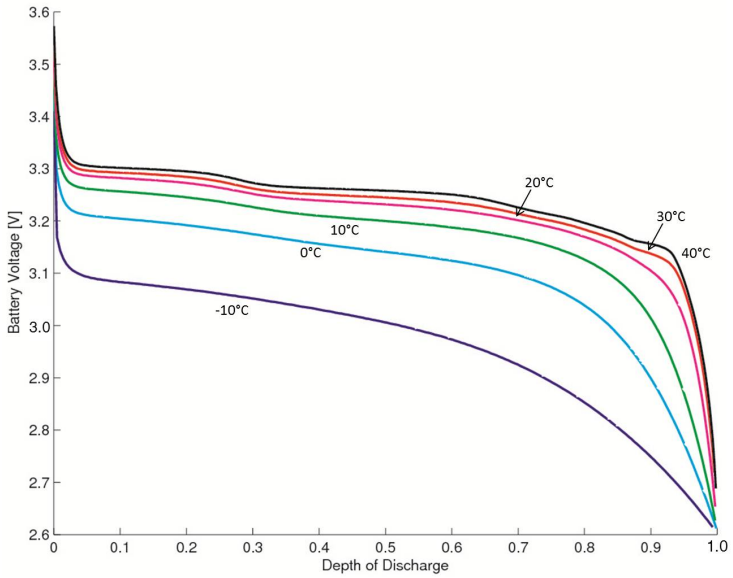

Figure 2: Effect of operating temperature on the discharge curve of the test battery at 0.5C constant current discharge

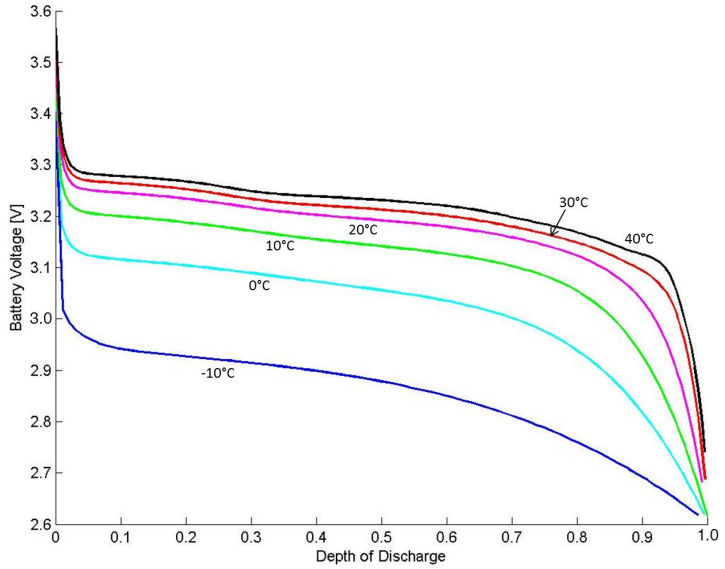

Figure 3: Effect of operating temperature on the discharge curve of the test battery at 1C constant current discharge

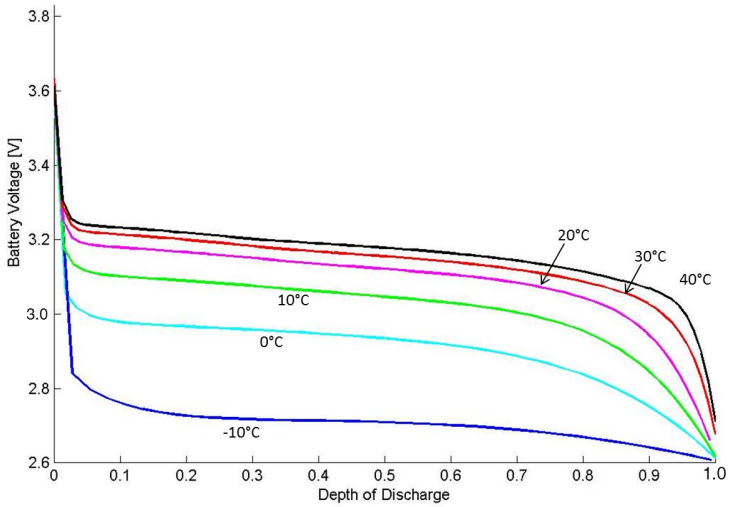

Figure 4: Effect of operating temperature on the discharge curve of the test battery at 2C constant current discharge

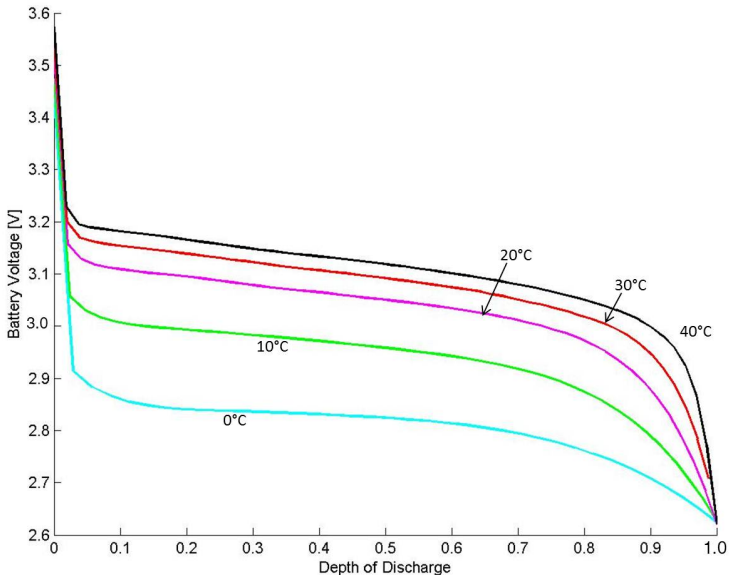

Figure 5: Effect of operating temperature on the discharge curve of the test battery at 3C constant current discharge

Appendix B: Effect of Discharge Rate on Battery Heat Generation

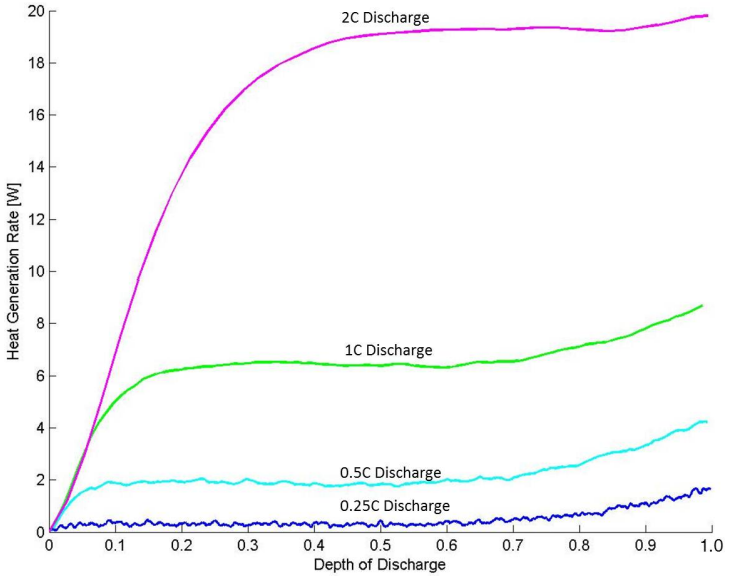

Figure 6: Effect of battery discharge rate on the heat generation profile of the test battery at an operating temperature of -10°C

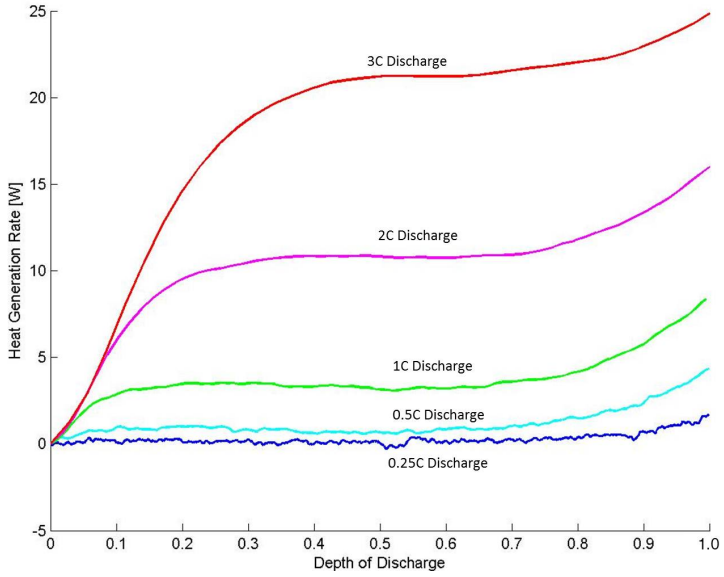

Figure 7: Effect of battery discharge rate on the heat generation profile of the test battery at an operating temperature of 0°C

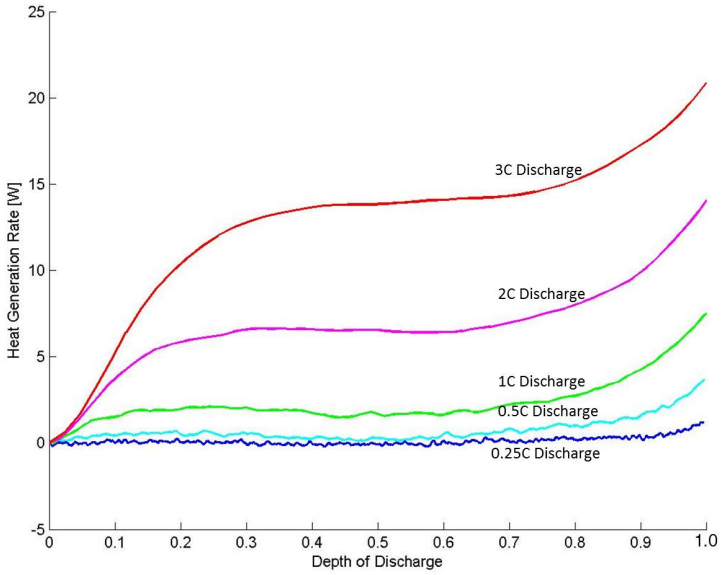

Figure 8: Effect of battery discharge rate on the heat generation profile of the test battery at an operating temperature of 10°C

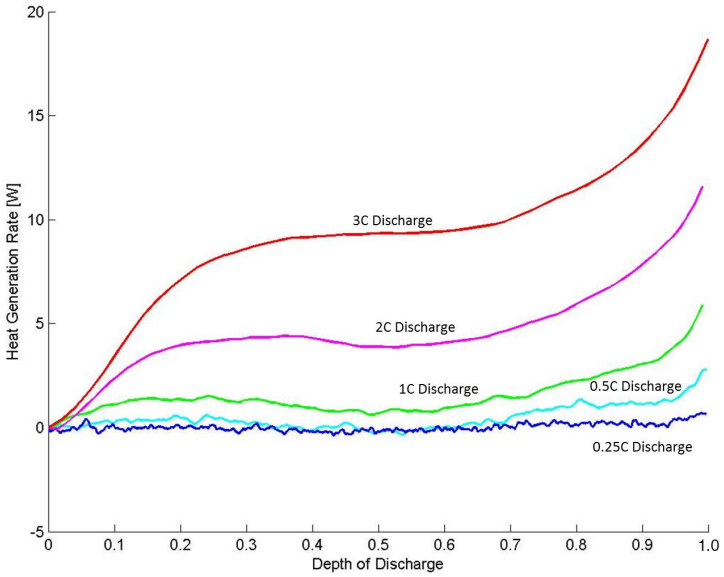

Figure 9: Effect of battery discharge rate on the heat generation profile of the test battery at an operating temperature of 20°C

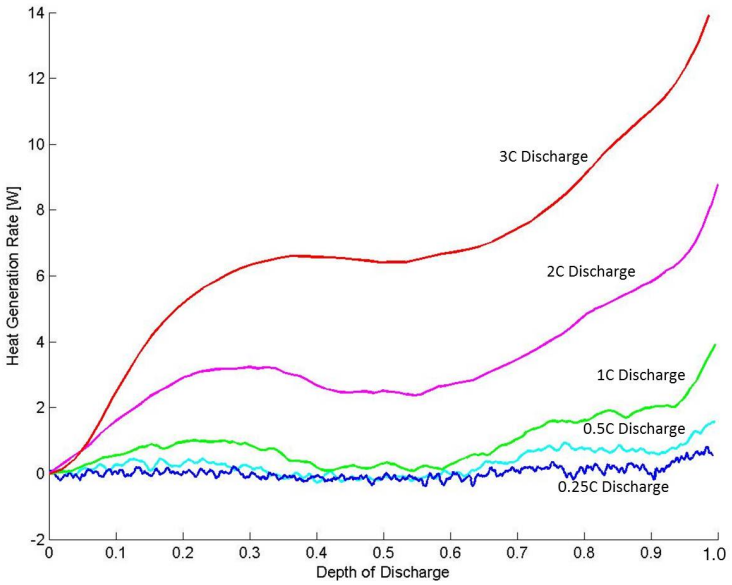

Figure 10: Effect of battery discharge rate on the heat generation profile of the test battery at an operating temperature of 30°C

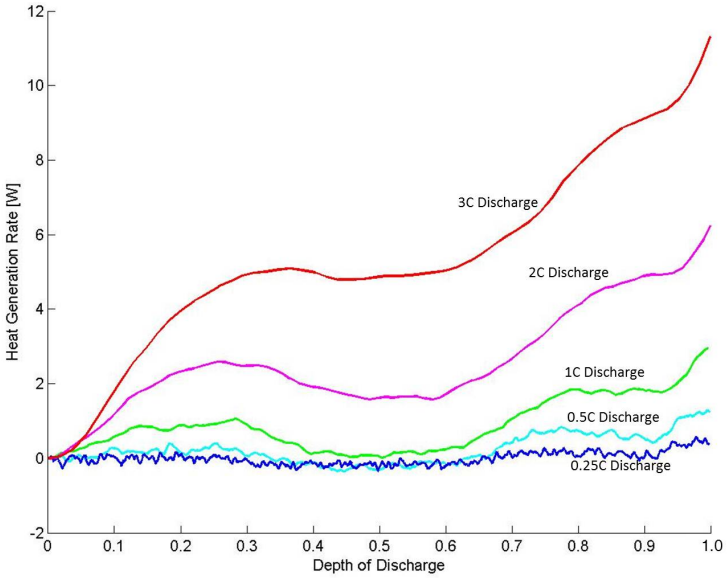

Figure 11: Effect of battery discharge rate on the heat generation profile of the test battery at an operating temperature of 40°C

Appendix C: Effect of Operating Temperature on Battery Heat Generation

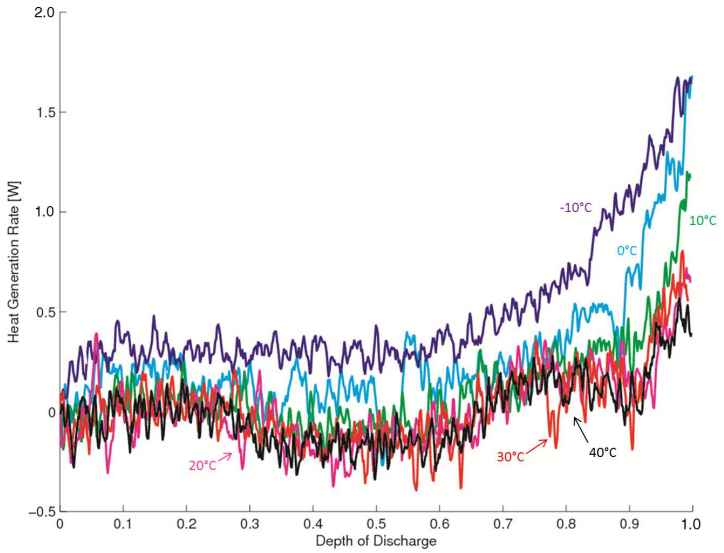

Figure 12: Effect of operating temperature on the heat generation profile of the test battery at 0.25C constant current discharge

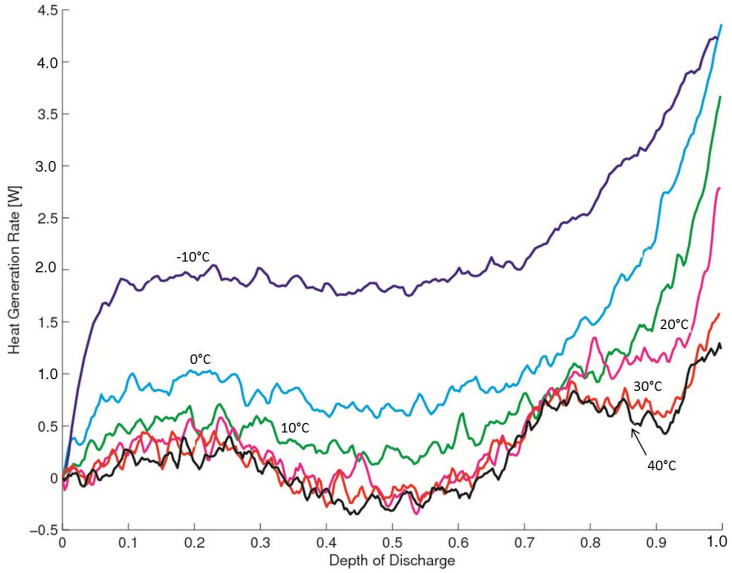

Figure 13: Effect of operating temperature on the heat generation profile of the test battery at 0.5C constant current discharge

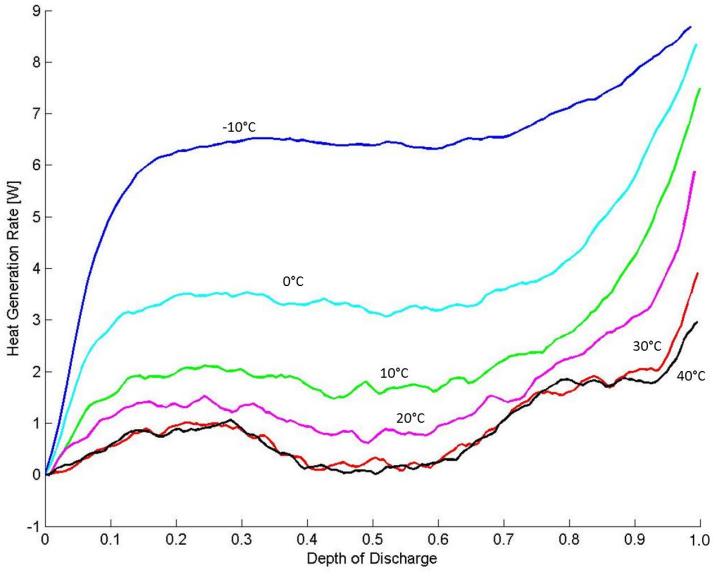

Figure 14: Effect of operating temperature on the heat generation profile of the test battery at 1C constant current discharge

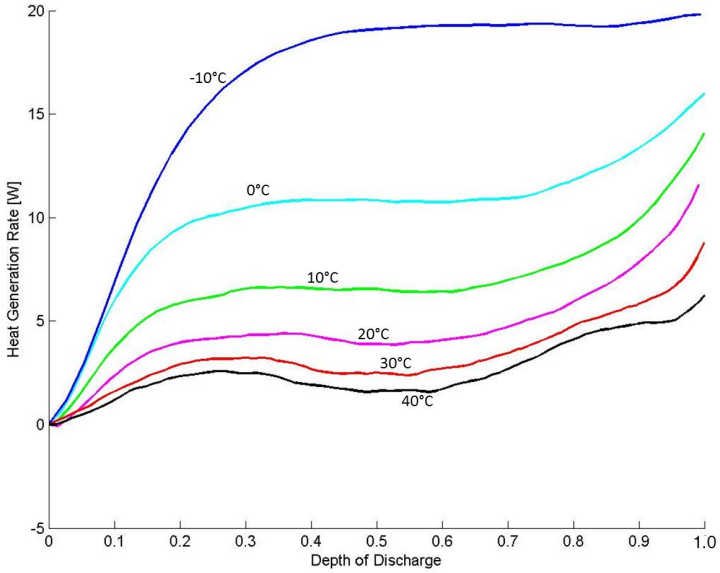

Figure 15: Effect of operating temperature on the heat generation profile of the test battery at 2C constant current discharge

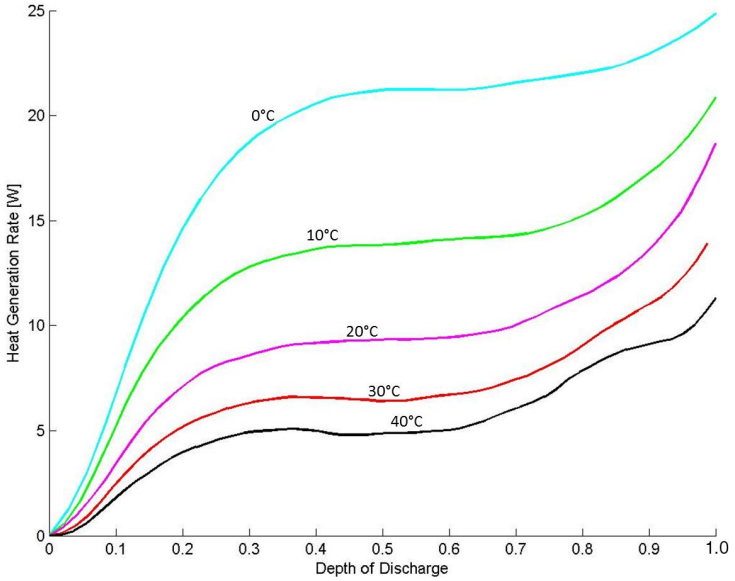

Figure 16: Effect of operating temperature on the heat generation profile of the test battery at 3C constant current discharge